

Potassium in the Galactic thin and thick discs

Carina Norregaard

Lund Observatory
Lund University



2018-EXA138

Degree project of 15 higher education credits
June 2018

Supervisor: Thomas Bensby

Lund Observatory
Box 43
SE-221 00 Lund
Sweden

Abstract

To understand the evolution of our galaxy, the chemical abundance patterns and trends within the stars of the different regions are explored. The process of synthesizing these elements reveals key details about the way the stars and, therefore, the galaxy formed.

This project focused on the element potassium, K, and specifically its absorption line 7699 Å. The local thermodynamic equilibrium (LTE) departures into non-local thermodynamic equilibrium (NLTE) must be taken into account, as potassium is highly affected. At first, synthetic spectra were applied to calculate the potassium abundances, but the NLTE effects were too strong, so equivalent width measurements were taken instead. To account for the NLTE effects, a table of NLTE corrections with corresponding stellar parameters was interpolated through with the data from 714 F and G dwarf stars in the Solar neighborhood. The tabulated NLTE corrections and stellar parameters were first analyzed to notice any outstanding trends. Then the interpolated corrections were analyzed against the same parameters. A dependence on temperature, surface gravity, and micro-turbulence was found. These corrections were then applied to the potassium abundances.

Using the corrected potassium abundances, ratios were taken between K and Fe, Mg, Ti, and iron-peak elements as well as r- and s- process elements. The [K/Fe] plot revealed an initially increasing and then decreasing trend, as the [Fe/H] increased. This showed behavior dissimilar to α elements. However, the [K/Mg] trends revealed a slightly increasing trend leading to a flat trend, with little scattering, indicating a potential link to the production site of α elements, type II SNe. In addition, [K/Mn] also had an increasing and then decreasing trend, owing most likely to the production of Mn in type Ia SNe. Furthermore, [K/Eu] revealed a flat trend, linking K again to production in type II SNe, where Eu is produced.

Amongst these [K/X] trends, a clear distinction was noticeable between trends of the thin and thick discs. The thick disc stars in the more metal poor regions of the plots were showing increasing trends of the [K/Fe] and [K/Mg] ratios, while the thin disc stars showed either flat or decreasing trends at the higher metallicity regions.

Populärvetenskaplig beskrivning

Nyfikenhet om stjärnorna och galaxerna runt om oss har fascinerat civilisationer i tusentals år. Rörelsen, ljuset, och mönster av himlakroppar har studerats av astronomer som försöker förstå universum och dess utveckling. En fascinerande aspekt av studien av ljuset som emitteras från avlägsna stjärnor är att man observerar det förflutna. Dessutom är det detta ljus och strålning som flyr stjärnorna som bär värdefull information, vilket avslöjar stjärnornas sammansättning och stjärnpopulationers utvecklingshistoria. Den data och kunskap som spektroskopi erbjuder är därför avgörande för att skapa en grundlig och djupgående förståelse av vår galax, Vintergatan, och i slutändan vårt universum.

Spektroskopi används fr att observera det ljusmönster som stjärnor sänder ut, och som avslöjar viktiga egenskaper hos stjärnan. Stjärnspektra uppvisas absorption såväl som emissionstoppar vid vissa våglängder beroende på vilka grundämnen som är närvarande i stjärnans atmosfär. Topparnas, eller dalarnas, egenskaper, såsom djup, bredd och position, beror på faktorer som temperatur, ytgravitation, och mikro- och makroturbulens. Kopplingen mellan sådana fenomen och deras effekter på det utsända spektrumet analyseras för att bestämma stjärnornas egenskaper. Exempelvis tenderar högre temperaturer att påverka spektrallinjernas bredd och vingar, och ytgravitationen påverkar den relativa styrkan hos linjer av olika jonisationsgrad. En noggrann analys av spektrallinjerna avslöjar därför kritiska egenskaper hos stjärnan.

Förutom att man observerar formen av spektrallinjer anger deras position och mönster de grundämnen som är närvarande. Spektrallinjerna fungerar som fingeravtryck, eftersom varje grundämnets linjer har specifika våglängder av ljus som den kan avge. Ymnigheten av dessa grundämnen kan hjälpa till att bestämma stjärnans ålder och dess ursprung. Istället för att bara analysera en stjärna åt gången, kan det vara mycket mer värdefullt att titta på grupper eller hopar av stjärnor eftersom de skapades samtidigt och borde ha liknande sammansättningar. På detta sätt kan en rad stjärnmassor och luminositeter undersökas. Dessutom kan man jämföra den kemiska sammansättningen och styra forskningen mot stjärnhopens, eller stjärnpopulationens, ålder och utveckling.

Att observera dessa grupper av stjärnor är särskilt användbar när man studerar vår egen galax, Vintergatan, eftersom den innehåller två definierade skivor av stjärnor, två olika stjärnpopulationer. Om Vintergatan kunde ses utifrån och från sidan så skulle man kanske kunna se en tunnare skiva av stjärnor som ligger inbäddad i en tjockare. Stjärnorna som finns inom dessa två skivor har även de olika egenskaper. Stjärnorna i den tjocka skivan har visat vara äldre stjärnor av lägre metallicitet, vilket betyder lägre ymnigheter av grundämnen som är tyngre än väte och helium. Den tunna skivan har å andra sidan stjärnor som är yngre än de i den tjocka skivan innehåller också större mängder av de tyngre grundämnena. Medan dessa trender och egenskaper hos skivorna är någorlunda kända, är det fortfarande oklart hur de har bildats och utvecklats.

Detta projektarbete, som fokuserar på spektrallinjerna som produceras av kalium i 714 stjärnor i Vintergatans tunna och tjocka skivor, är ett grundläggande exempel på den forskning och analys som utförs i dagens Vintergatsforskning. Mängden, eller ymnigheten, av grundämnen mäts och analyseras med målet att bestämma stjärnornas kemiska sam-

mansättning och stjärnpopulationernas evolutionära väg. Studier av individuella grundämnen, med hjälp av nyare och mer exakta data och teknik, kan en klarare och mer välbestämd förståelse av vår galax.

Contents

1	Introduction	4
2	Method	7
2.1	Stellar sample	7
2.2	Analysis	7
2.2.1	Abundance measurement	7
2.2.2	Potassium lines	8
2.2.3	Line synthesis	8
2.2.4	NLTE	9
2.2.5	Equivalent widths	10
2.2.6	NLTE corrections	11
2.2.7	Uncertainties	16
3	Results	17
3.1	Potassium NLTE corrections	17
3.2	K trends in the thin and thick discs	19
3.3	Discussion	24
3.4	Summary and conclusion	25
A	NLTE K abundances and corrections	29

List of Figures

2.1	Synthetic spectra for HIP80 and HIP305 showing the line profile widening and not deepening. Even though it says Li, these measurements were done with K, the program was previously used for Li.	9
2.2	The potassium line blended with a telluric pair as seen by the merged line.	11
2.3	Stellar parameter table NLTE corrections plotted against $T_{eff}(K)$, the solid lines correspond to a micro-turbulence of 1.0 km/s, the dotted lines to 2.0 km/s and the dashed lines to 3.0 km/s (Takeda et al. 2002).	12
2.4	Stellar parameter table NLTE corrections plotted against $[Fe/H]$, where the solid line represents a micro-turbulence of 1.0 km/s, the dotted line a micro-turbulence of 2.0 km/s, and the dashed line a micro-turbulence of 3.0 km/s (Takeda et al. 2002).	14
2.5	Stellar parameter table NLTE corrections plotted against $\log(g)$ for a given metallicity, where the solid line represents a micro-turbulence of 1.0 km/s, the dotted line a micro-turbulence of 2.0 km/s, and the dashed line a micro-turbulence of 3.0 km/s Takeda et al. (2002).	15
3.1	Calculated NLTE corrections plotted against the stellar parameters	18
3.2	Potassium abundances without and with NLTE corrections plotted against $[Fe/H]$	19
3.3	(a) NLTE corrected potassium abundance plotted against $[Fe/H]$ with a distinction of the thin and the thick discs, (b) $[Mg/Fe]$ plotted against $[Fe/H]$	20
3.4	(a) $[K/Mg]$ plotted against $[Mg/H]$, (b) $[K/Mg]$ plotted against $[Fe/H]$	20
3.5	(a) $[K/Ti]$ plotted against $[Ti/H]$, (b) $[K/Ti]$ plotted against $[Fe/H]$	21
3.6	(a) $[K/Sc]$ plotted against $[Fe/H]$, (b) $[K/V]$ plotted against $[Fe/H]$, (c) $[K/Mn]$ with NLTE corrections plotted against $[Fe/H]$, (d) $[K/Co]$ with NLTE corrections plotted against $[Fe/H]$	22
3.7	$[K/Sr]$, $[K/Zr]$, $[K/La]$, $[K/Ce]$, $[K/Nd]$, $[K/Sm]$, and $[K/Eu]$ plotted against $[Fe/H]$	23

List of Tables

A.1	Table of the final K abundances and their NLTE corrections	29
-----	--	----

Chapter 1

Introduction

Studying the chemical abundances of stars in different regions of galaxies allows for an insight into the evolution and creation of the galaxy itself. The chemical abundances, alongside the timescale, position within the galaxy, and the stellar parameters, reveal patterns that can guide our understanding. These patterns become crucial when considering our own Milky Way Galaxy, and its potential origins.

The process of generating and synthesizing new elements as well as creating stars is an ongoing cycle. The elements comprising the galactic gas are the light elements of H, He, and Li, which are also the elements present in the primordial gas (Mushotzky 2015; Samland 1998). The elements heavier than these are referred to as the metals, and are generated in stars. All the elements up to Fe are able to be produced in the core of the stars when there is enough energy to overcome the threshold energy to fuse nuclei. When the galactic gas comes together to form a star, it is then able to create these new heavier elements out of its existing atoms, or through nucleosynthesis. Then, as the star ages, the enriched material is dispersed into the interstellar medium through various means. The common processes leading to the ejection of this material are mass loss and supernovae (SNe). The cycle begins again, where the gas forming the new stars has been enriched with heavier metals from the older stars. As the cycle continues, the stars generated as well as the interstellar medium become more enriched with heavier elements (Mushotzky 2015). In this way, the chemical evolution of the galaxy can be traced through the differing element abundances.

In addition to tracing the chemical evolution of the galaxy through the element abundances, the data can also reveal the influence of events such as type II and type Ia SNe. The type II core collapse SNe occur in massive stars and are one of the main generators of the α elements, like C, O, Ne, Mg, Si, S, Ar, and Ca. They are induced usually around 10^7 yr after the stars have formed (Mushotzky 2015). In contrast, the type Ia SNe occur in binary systems with the presence of a carbon-oxygen white dwarf (Matteucci 2016). The explosion is caused primarily by dynamical and thermal instabilities (Prialnik 2010). These type Ia SNe do not produce the α elements, but they do create Fe. They tend to take place later than 10^8 yr after the stars had formed. Applying this knowledge to the resulting element abundance ratios exposes the links between the production of elements.

In other words, it can show if the elements are synthesized during the same events or through events occurring at different times and in different spaces.

When observing most of these galaxies edge-on, a distinction can be made in terms of stellar population in a thin and thick disc. After Gilmore & Reid (1983) published a paper that began to apply this thin and thick disc distinction to the Milky Way Galaxy, research was inspired to characterize the differences of the stars present in the two discs. Exploring and elaborating on patterns concerning the metallicity, abundance, and other parameters with continuous newly acquired data enables newer and more accurate hypotheses to be developed. Such hypotheses outlining the formation of the thick disc include phenomena such as the accretion of galaxy satellites, implying extragalactic origin for the thick disc stars. Another is the heating of thin discs, occurring at a range of timescales from fast to over the lifetime of the galaxy (Minchev et al. 2012).

Exploring the origins of the Milky Way Galaxy leads to the examination of the stars within the thin and thick disc separately. In this way, finding trends linking the stars within each respective disc can direct and focus research. The thick disc holds the older and metal-poor stars, meaning the thin disc is comprised of relatively younger stars with higher metallicities. The analysis of the chemical abundances is therefore conducted in depth to fully comprehend the principal characteristics of these stellar populations.

One of the main methods of examination of these stars is through spectroscopy, which reveals a wealth of information simply from the emitted light from the stars. The resulting absorption lines create fingerprints identifying the elements present within the star. The importance of the placement of the observational instrument becomes evident when observing data collected from an Earth based instrument, as the effect of the Earth's atmosphere on the spectra can produce additional lines known as telluric lines.

This project attempts to explore the origins of the thin and thick disc through one element, potassium. This element was chosen as there is limited knowledge about its role in the galactic evolution, both theoretically and observationally (Takeda et al. 2002). Potassium is typically created through the burning of lighter elements. The main event producing potassium from a lighter element is the burning of oxygen in type II supernovae (Shimansky et al. 2003). Furthermore, it is a low ionization energy element (Zhang et al. 2006a) that is known to be collision dominated (Zhao et al. 2016). Even though potassium is collision dominated, the assumption of local thermodynamic equilibrium (LTE) can not be applied as it would produce inaccurate potassium abundance values (Shimansky et al. 2003). The cause of the LTE departures into non-LTE (NLTE) environments is the sensitivity of potassium to over-recombination (Shimansky et al. 2003; Zhao et al. 2016). Therefore, it is the ionization balance of the potassium energy levels that contributes to the deviations from LTE, compelling the method of analysis to cater towards the resulting effects on the spectra from the stars.

After exploring the possible potassium lines available for analysis, the 7699 Å line was chosen. A database of the spectra of 714 F and G dwarf stars was investigated, with a focus on the 7699 Å line. Taking into consideration the need to account for the NLTE effects, the equivalent width method was chosen as a means of analysis. Since the abundances were found under the LTE assumption, a table of stellar atmosphere parameters from Takeda

et al. (2002) with NLTE corrections were applied. These corrections then allowed for the more accurate potassium abundances to be compared to the parameters of the stars in the thin and thick disc.

Chapter 2

Method

2.1 Stellar sample

The stellar sample analyzed in this project was collected from Bensby et al. (2014). The data includes a total of 714 solar neighborhood F and G dwarf stars and subgiant stars. The elements observed included O, Na, Mg, Al, Si, Ca, Ti, Cr, Fe, Ni, Zn, Y, and Ba. The spectra were recorded with the following instruments: MIKE, FEROS, HARPS, UVES, SOFIN, and FIES. The typical signal-to-noise ratio of the spectra is as high as 200. This sample selection was chosen by the kinematics of the stars, such that they had Gaussian velocity distributions and that they inhabit a certain portion of the of the Solar neighborhood. These properties were chosen to be in between thin and thick disc stars. In addition, they were chosen to trace the metal-poor limit of the thin disc, the metal-rich limit of the thick disc and the metal-poor limit of the thick disc (Bensby et al. 2014).

The stellar parameters, chemical abundance ratios, ages, and kinematics of all 714 stars were gathered from table C.3 in Bensby et al. (2014). Furthermore, this table contained the corresponding calculated uncertainties for parameters such as $[\text{Fe}/\text{H}]$, $\log g$, micro-turbulence, as well as for the chemical abundance ratios. The data concerning the odd-Z iron peak elements was collected from Battistini & Bensby (2015), including the line synthesis of the Sc, V, Mn, and Co lines. The data for the r- and s- process elements was retrieved from Battistini & Bensby (2016), which also contained line synthesis data but for the elements of Sr, Zr, La, Ce, Nd, Sm, and Eu.

From the stellar spectra of the 714 stars, the potassium lines are added to the data and used to uncover additional details about the evolution of the thin and thick disc.

2.2 Analysis

2.2.1 Abundance measurement

To measure the abundance of an element from the stellar spectra, there are two main methods used. The first is the line synthesis method, where synthetic spectra are fitted to

the data to measure the abundance. The second method is the equivalent width method, where the absorption lines are fit with a Gaussian or Voigt distribution to extract the equivalent width of the line. For both of these methods, detailed information is required on the behavior of the atoms of the element of interest. Vienna atomic line database (VALD) information is gathered and applied to the program calculating the abundances. The VALD data reveals the oscillator strength of the atomic energy transitions, or the log gf values, which reflects the probability of an excitation or de-excitation and affects the strength of a line. In addition, the VALD data records the damping parameters of the absorption lines. These damping parameters affect the width of the produced lines and include the Van der Waals and Stark collisional broadening. In addition, to calculate the abundances, model stellar atmospheres are needed, which in this case are the same as those presented in Bensby et al. (2014).

2.2.2 Potassium lines

To begin the analysis of the stellar spectra, a strong identifying absorption line for potassium was chosen, at 7699 Å. Other potassium lines exist at 6938 Å and 5802 Å (Zhang et al. 2006a), however these were not strong enough to evaluate clearly. In addition, another potassium line appears at 7664 Å but is typically too blended with O₂ telluric lines to measure (Zhao et al. 2016; Takeda et al. 2002). An important consideration in the analysis of the absorption lines is the presence of hyperfine splitting, but for this 7699 Å K I line it can be neglected (Zhang et al. 2006a). Before measurements were taken, atomic information and details were gathered to accommodate the properties of potassium. This included querying valuable information about the atomic parameters of potassium from VALD, (Kurucz 2004, 2007, 2008, 2010, 2012, 2013, 2014; Barklem & Aspelund-Johansson 2005; Barklem et al. 2000; O'Brian et al. 1991; Fuhr et al. 1988; Ralchenko et al. 2010; Raassen & Uylings 1998). The requested information outlined the elements corresponding to characteristic peak wavelengths in the range of wavelengths indicated, as well as damping parameter values and astrophysical gf values.

2.2.3 Line synthesis

The first method of analysis chosen was the line synthesis. The synthetic spectra method generates spectra to fit the collected data, however, it does not take into consideration the effects of NLTE and even as the code was manipulated to try to fit the spectrum data, the synthetic spectra did not match the data, as shown in figures 2.1(a) and 2.1(b). As parameters, such as abundance, of the program were altered to attempt to fit the data, the synthetic line profiles only grew wider and wider and were not able to reach the depth of the absorption line. These results revealed the extent of the severe effects of the NLTE on the potassium line, and directed the analysis to a different form of measurement, equivalent widths. The NLTE effects on the potassium line were confirmed when Takeda et al. (2002) was consulted.

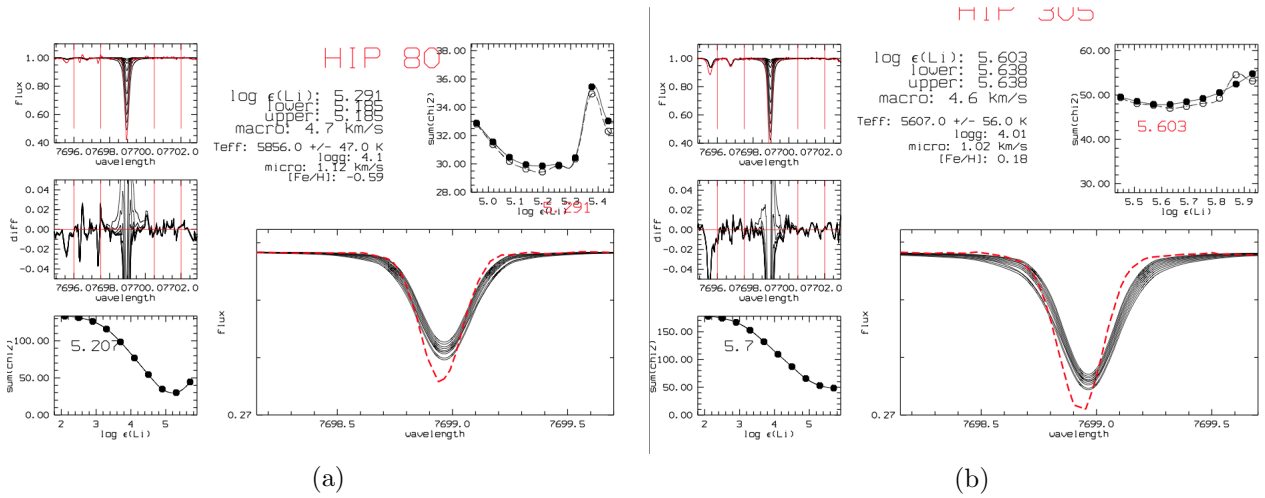


Figure 2.1: Synthetic spectra for HIP80 and HIP305 showing the line profile widening and not deepening. Even though it says Li, these measurements were done with K, the program was previously used for Li.

2.2.4 NLTE

After realizing the influence of the NLTE and LTE assumptions on the K line at 7699 Å, the basis of these concepts were explored. Takeda et al. (2002) also show the effects of NLTE on this K line. In the modeling of stellar photospheres, the LTE and NLTE assumptions and approximations made are crucial in understanding and analyzing the spectral data from the stars. A useful concept is the black-body, where the emitted and absorbed radiation develop an equilibrium. This black-body is in thermodynamic equilibrium as long as the temperature remains constant. Relating this concept to the photosphere of a star, observing the lowest depths reveals that little radiation is able to escape the photosphere. This behavior is due to the photons being re-absorbed close to where they were emitted. The main parameter causing this effect is a large optical depth, τ_ν , which is known as optically thick,

$$\tau_\nu = \int \alpha_\nu ds, \quad (2.1)$$

where α_ν represents the extinction-coefficient parameter of the star. From the relation (2.1) it is clear that if τ_ν is large, that α_ν is also large, signifying a large extinction, or re-absorption of radiation. In this deep area of the photosphere, the LTE assumptions can therefore be applied to maintain the benefits of this equilibrium, as the medium is given by the local temperature. Such assumptions include allowing the distribution of the particle velocities to be Maxwellian, and using the Saha-Boltzman distribution for the excitation and ionization states (Kubát 2014). Furthermore, to remain in an LTE approximation, the main process dominating the excitations must be collision based. The ionization equation for such a process is given by the following (Gray 2005),

$$\frac{N_1}{N_0} P_e = \frac{(2\pi m_e)^{3/2} (kT)^{5/2} 2u_1(T)}{h^3 u_0(T)} e^{-I/kT}, \quad (2.2)$$

where $\frac{N_1}{N_0}$ represents the ratio of ionized to neutral atoms and $\frac{u_1}{u_0}$ represents the ionized to neutral partition functions. As can be seen, this expression is dependent on the temperature.

In addition, the source function while within LTE can be approximated by a Planck function, $S_\nu = B(T)$. The Planck function applied here is used to solve the transport equation for the star's atmosphere where these LTE approximations are valid.

As the depth into the photosphere decreases, the photons are less likely to be re-absorbed near where they were emitted, and the concept of local thermodynamic equilibrium is no longer valid. Here, in the higher layers, an NLTE application must be implemented. In these regions, the excitations are no longer collision based, but are radiation dominated, which clearly emphasizes the non-local property. Whereas previously the source function could be approximated to a Planck function, in NLTE regions the exact source function must be used, with exact emissivity and extinction coefficients (Kubát 2014). However, the Maxwell distribution for the particle velocities remains valid. Therefore, in NLTE, instead of focusing on thermodynamic equilibrium, the attention shifts to kinetic equilibrium, where the radiative transport equation is solved using the exact source function.

In this case with potassium, even though it is collision based, implying LTE, the ionization balance of its energy levels render the Saha-Boltzman distribution inaccurate. While potassium does not immediately direct analysis to focus on NLTE since it is not radiation dominated, it still demands the departures from LTE to be applied, requiring NLTE corrections. Therefore, the analysis method was revised to take this into consideration.

2.2.5 Equivalent widths

The second commonly used method in spectral analysis is Equivalent Width (EW) measurement. To do so, a Voigt fit was placed over the desired absorption line in the spectra and the EW value was extracted into a table to later use to calculate the potassium abundance, initially under LTE assumptions. The Voigt fit was used because it is the convolution of the Lorentzian and Gaussian distributions, where the wings of the Lorentzian and the body of the Gaussian are applied. The SPLOT function in IRAF was used to measure these EWs. Each potassium line EW around 7699 Å was manually measured applying the Voigt fit, which allowed for a detailed scan of the data to ensure it useful. This revealed around 80 of the 714 sets of data were not useful due to line blending. The principal origin of the line blending was the presence of telluric lines. The characteristic that affected these 80 stars, causing the potassium line to blend with the telluric lines was their radial velocity, which shifts the absorption lines.

Since many observations of stellar spectra are made from Earth, the effect of the Earth's atmosphere on the data must be taken into account. A common phenomenon appearing on

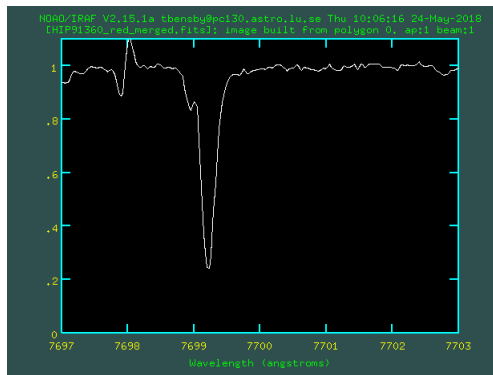


Figure 2.2: The potassium line blended with a telluric pair as seen by the merged line.

the observed spectra are telluric lines. These lines are created as a result of the interaction between the incoming light and the molecules comprising the atmosphere. The temperature at which these molecules remain is of the order 275 K (Adelman et al. 1996), which allows their atoms to absorb incident radiation and cause the telluric lines. These molecules include O_2 , N_2 , and Ar. The telluric lines appearing as result of the interaction tend to affect the red and infrared section of the spectra, which is exactly the location of the chosen potassium line (Adelman et al. 1996). Furthermore, an identifiable characteristic is the occurrence of pairs of telluric lines. An example of blending with telluric lines can be seen in figure 2.2. The effect of the blended telluric lines was a deeper absorption line and as well as a shift of position. At the risk of skewing the data, these heavily and obviously blended lines were omitted from the analysis.

2.2.6 NLTE corrections

After calculating the potassium abundances for the valid datasets, the next step was applying the NLTE corrections. Since the corrections depended on effective temperature, surface gravity, metallicity, and micro-turbulence, a table of stellar atmosphere parameters was used to interpolate through with the actual stellar parameters and determine the corresponding exact NLTE correction to be applied. The table of these stellar atmospheres parameters and NLTE correction was found from Takeda et al. (2002). The tables are a set of three files, each file pertaining to values for a micro-turbulence of either 1.0 km/s, 2.0 km/s, or 3.0 km/s. Three sample LTE potassium abundances are used for each set of temperature, metallicity, and surface gravity values. The effective temperature ranges from 4500 K to 6500 K, the surface gravity ranges from 0.0 to 5.0, and the metallicity ranges from 0 to -3. To get a sense of the dependency of the corrections on the stated stellar parameters, a series of plots were made reflecting the relationships between the corrections and the stellar parameters. The first set of plots, figures 2.3(a) to 2.3(e), reflect the trends between the NLTE corrections and the temperature.

Observing these plots reveals the sensitivity of the corrections to temperature in the lower ranges of the surface gravity. With a surface gravity of 1.0 and $[Fe/H]=0$, the

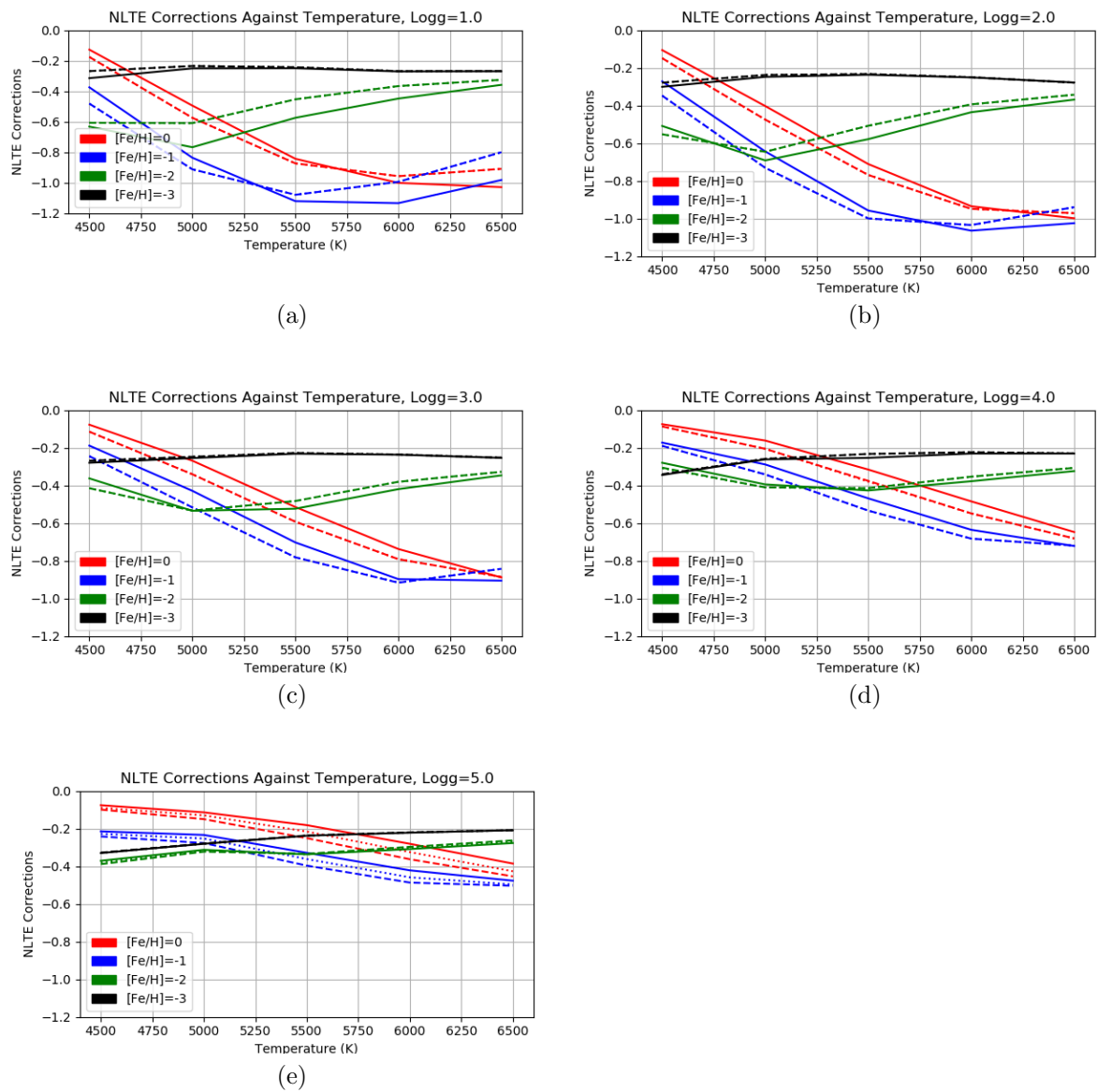


Figure 2.3: Stellar parameter table NLTE corrections plotted against $T_{eff}(K)$, the solid lines correspond to a micro-turbulence of 1.0 km/s, the dotted lines to 2.0 km/s and the dashed lines to 3.0 km/s (Takeda et al. 2002).

corrections span values from -0.1 to -1.0. Comparing the same metallicity with a surface gravity of 5.0, the corrections only span values from -0.05 to -0.4. Furthermore, another trend is evident regarding the corrections pertaining to the different metallicities. For each surface gravity value, the $[\text{Fe}/\text{H}] = 0, -1$ tend to decrease, while the $[\text{Fe}/\text{H}] = -2, -3$ tend to increase or remain constant.

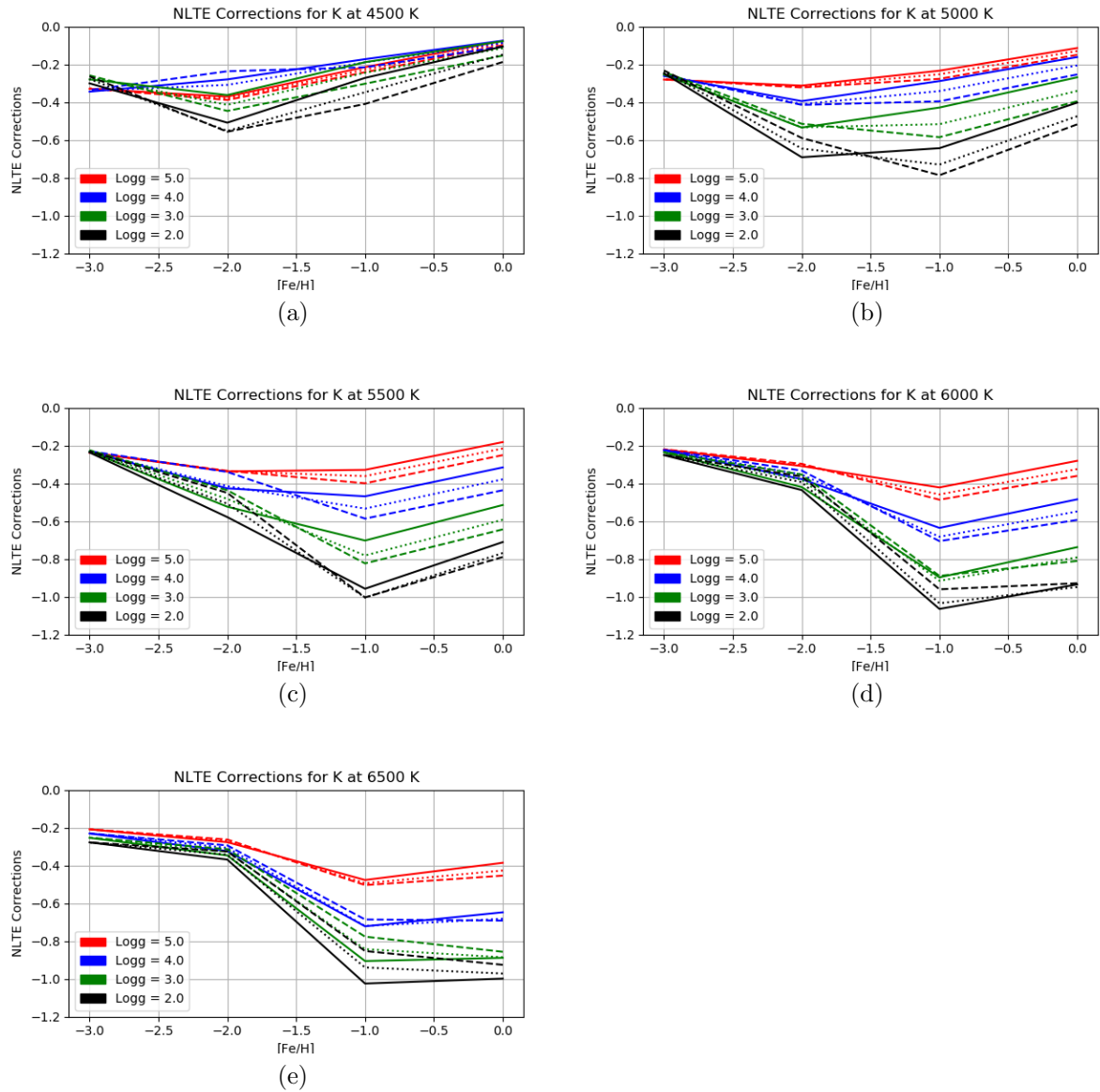


Figure 2.4: Stellar parameter table NLTE corrections plotted against $[\text{Fe}/\text{H}]$, where the solid line represents a micro-turbulence of 1.0 km/s, the dotted line a micro-turbulence of 2.0 km/s, and the dashed line a micro-turbulence of 3.0 km/s (Takeda et al. 2002).

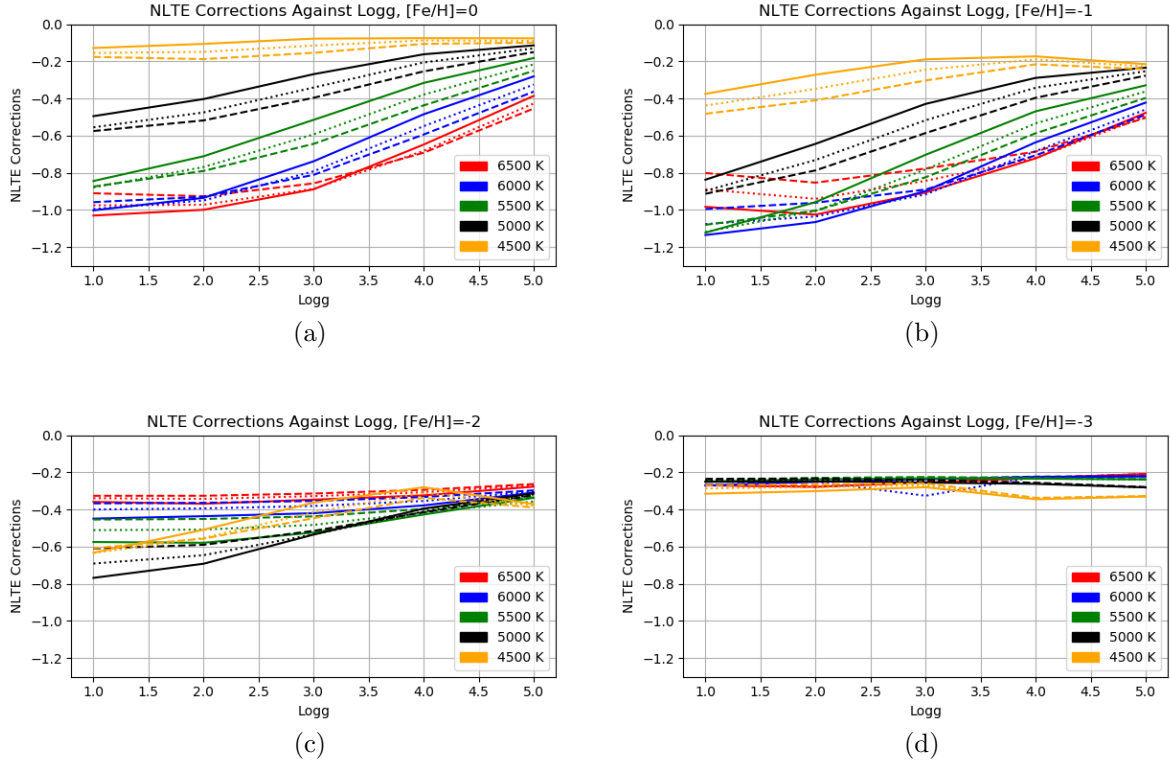


Figure 2.5: Stellar parameter table NLTE corrections plotted against $\log(g)$ for a given metallicity, where the solid line represents a micro-turbulence of 1.0 km/s, the dotted line a micro-turbulence of 2.0 km/s, and the dashed line a micro-turbulence of 3.0 km/s Takeda et al. (2002).

Figures 2.4(a) through 2.4(e) present the relationships between the corrections and the metallicity for a given temperature. Each graph distinguishes between the varying surface gravity values. As can be seen, as the temperature increases, the corrections span a larger range of values. In addition, as the metallicity increases, the corrections first seem to decrease slightly before increasing.

Figures 2.5(a) through to 2.5(e) reflect the relationship between the NLTE corrections and the surface gravity of the stars for the given metallicity values. As can be seen, at $[\text{Fe}/\text{H}] = 0$ and -1 , the NLTE corrections for temperatures larger than 4500 K vary a lot with increasing surface gravity. At $[\text{Fe}/\text{H}] = -2$ and -3 , the corrections span a smaller range with increasing surface gravity.

These tables were then used to calculate the exact NLTE correction corresponding to each star. First, the form of the measured potassium abundances were converted from relative to the sun to absolute abundances by adding the non-corrected value of the Sun's abundance. Then the measured LTE abundances were interpolated through the tables to reach one correction value for each set of temperature, metallicity, and surface gravity val-

ues. The surface gravity values from table C.3 Bensby et al. (2014) were then interpolated through the Takeda et al. (2002) tables to reach one set of corrections for each temperature and metallicity. This procedure was repeated until only one correction value remained to interpolate between the three micro-turbulence files. This correction value was stored and applied to the original measured LTE potassium abundances. After these final corrected absolute abundance values were determined, the corrected Sun's abundance was subtracted to convert back to the relative form.

After calculating and applying the corrections to the potassium abundances, the analysis seeking trends and exploring the relationships between these abundances and several parameters was conducted. Initially, the [K/Fe] and [Fe/H] trends were observed before and after the corrections were applied. Then a distinction was made between the thin and thick disc stars to notice any differentiating patterns. Furthermore, potassium's relation to other elements was investigated, by plotting [K/X] by [Fe/H]. The elements included α , odd-Z iron peak, and r- and s- process elements.

2.2.7 Uncertainties

The errors applied to the [K/Fe], [K/Mg], and [Fe/H] values were calculated using the four observables associated with the main stellar parameters of temperature, micro-turbulence, surface gravity, and metallicity. Each observable has a corresponding error, which is taken as the uncertainty of the linear regression of the associated observable plot (Bensby et al. 2014; Epstein et al. 2010).

From the method of analysis conducted in this project, there are several steps that could have contributed to potential errors. These include the measurements of the EWs as the placement of the Voigt fit and continuum were done by hand, the placements could have shifted with each absorption line. This influences the subsequent abundance calculations. Furthermore, since the severity of the blended lines was measured by eye, some retained data may have telluric blending that was not obvious. This may have affected the abundance values. In addition, during the interpolation calculations of the NLTE corrections, the relationship within the respective parameters was assumed to be linear, which could have skewed the final correction values if the relationship were actually of some other form.

Chapter 3

Results

3.1 Potassium NLTE corrections

After investigating the trends present in the tables of the NLTE corrections and stellar parameters, they were used to determine the corresponding NLTE potassium corrections for the previously measured LTE abundances. To do so, the models were interpolated through using a Python script. The parameters guiding the interpolation were the effective temperature, the surface gravity, the metallicity, and the micro-turbulence values of the stars, found in table C.3 of Bensby et al. (2014). The resulting NLTE correction values for each star can be found recorded in table A.1, alongside the corrected abundances. The mean value of the corrections was -0.44.

Observing figures 3.1(a) to 3.1(e) reveals the trends between the calculated corrections and the parameters of the corresponding stars. Figure 3.1(a) represents the dependence of the corrections on the metallicity, which shows a constant trend, meaning little dependence. Figure 3.1(b) shows the relation between the corrections and the temperature, reflecting a clear decrease (or larger NLTE effect) as the effective temperature increases.

Figure 3.1(e) presents the relation between the corrections and the surface gravity. The corrections seem to decrease slightly between $\log g = 3.50$ and 4.25 and then increase slightly between $\log g = 4.25$ and 4.50 . These three trends agree with Zhang et al. (2006b) who states the same patterns. Figure 3.1(c) presents the dependence of the NLTE corrections on the LTE absolute potassium abundances. No clear trend is noticeable here, the thick disc stars tend to correspond to the lower K abundance values. Figure 3.1(d) reveals the relationship between the corrections and the micro-turbulence and shows an immediate decrease in the correction values with an increase of the micro-turbulence.

The Sun's uncorrected potassium abundance was 5.41, which was added to the LTE abundance values in the beginning of the analysis. To find the Sun's correction value, the same interpolation procedure was used, producing a correction of -0.33.

To get an overview of the data, two plots were made comparing the $[K/Fe]$ with $[Fe/H]$ before and after the NLTE corrections were made, shown by figures 3.2(a) and 3.2(b), respectively. Keeping in mind that the Sun's correction was -0.33 and the mean correction

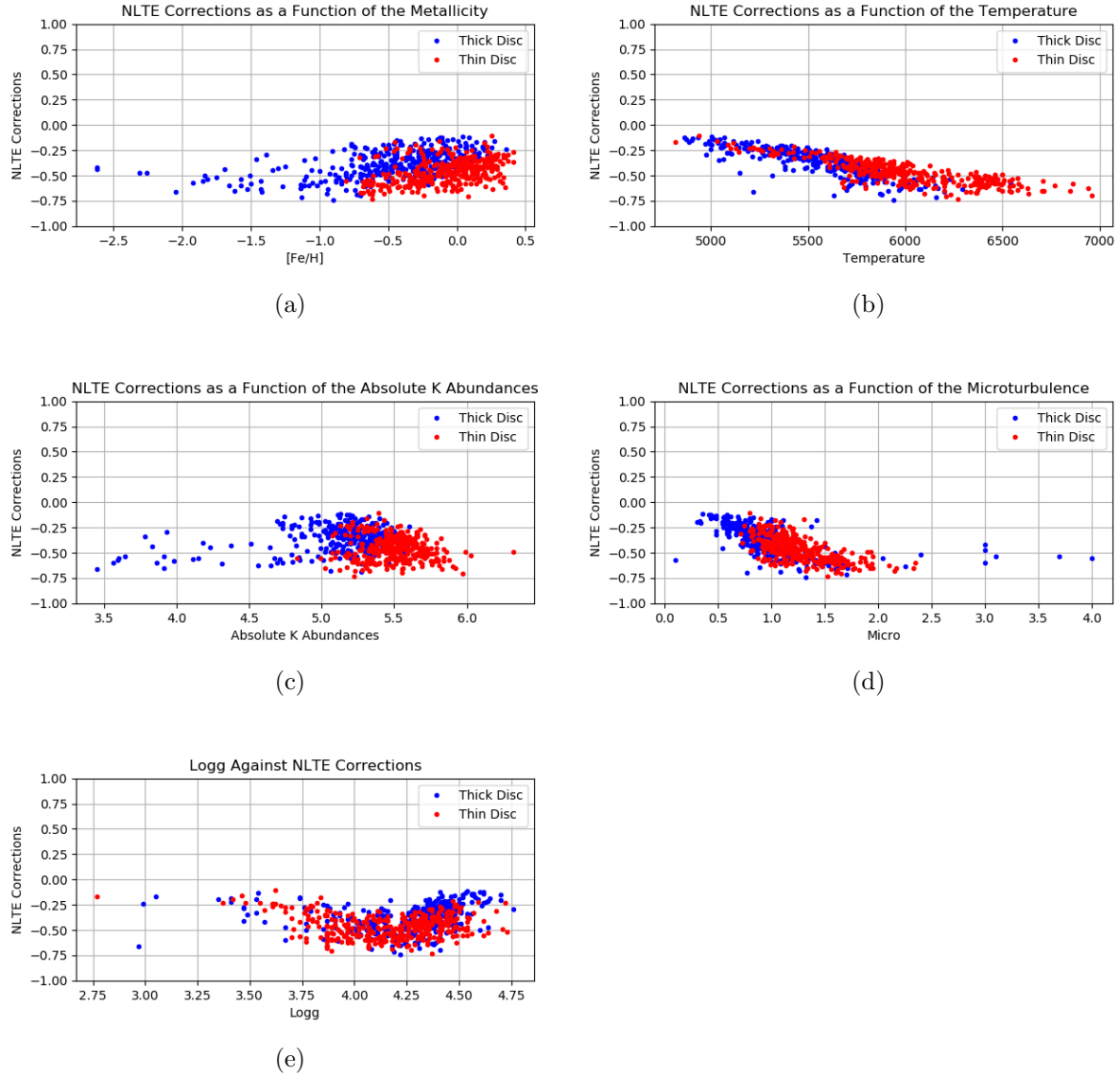


Figure 3.1: Calculated NLTE corrections plotted against the stellar parameters

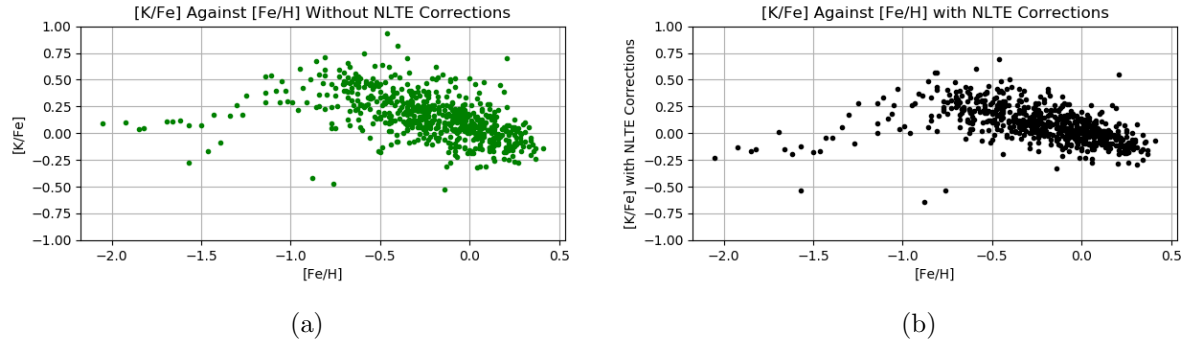


Figure 3.2: Potassium abundances without and with NLTE corrections plotted against $[\text{Fe}/\text{H}]$

value was -0.44 , it makes sense that the data points shift down slightly when the corrections are applied. Overall the trend remains similar, with an initial increase in the $[\text{K}/\text{Fe}]$ with $[\text{Fe}/\text{H}]$, and then a decrease starting around $[\text{Fe}/\text{H}] = -0.75$, which seems to match most closely to the model shown in Timmes et al. (1995) as they represent an initial increase as well. Moreover, after applying the NLTE corrections, there was less scatter in the data points, indicating better results after applying the corrections.

3.2 K trends in the thin and thick discs

Once the potassium abundances were corrected for the NLTE effects, they were used to compare to other elements present in the stars, as well as to investigate the differences between the thin and thick disc.

The next step was to look closer into the differences between the thin and thick disc. To distinguish between the thin and thick disc stars, the limiting age for the thin disc stars was set to be 8 Gyr, which left the thick disc stars to be those older than 8 Gyr. It is possible to identify the thin and thick disc stars through their stellar orbit radius variations as well as their kinematic properties, however their ages are a clearer distinguisher (Bensby et al. 2014).

The resulting plot is shown in figure 3.3(a). As shown, it is dominantly the thick disc stars in the metal-poor region, reflecting an increasing trend. It is interesting to compare K to an α element such as Mg. The $[\text{Mg}/\text{Fe}]$ against $[\text{Fe}/\text{H}]$ trend is shown figure 3.3(b). Here, the metal poor, thick disc stars maintain a relatively constant ratio between Mg and Fe, which is consistent with the production of Mg and Fe from type II supernovae. The decreasing trend in the more metal-rich region is also consistent with the ratio of production of Mg and Fe from type Ia supernovae, since Mg is not produced in type Ia SNe. Therefore, the differing trends of the metal-poor regions for these two elements prompts a further investigation.

Zhang et al. (2006b) agrees with the decreasing $[\text{K}/\text{Fe}]$ trend from $[\text{Fe}/\text{H}] = -1.0$ to 0.2 .

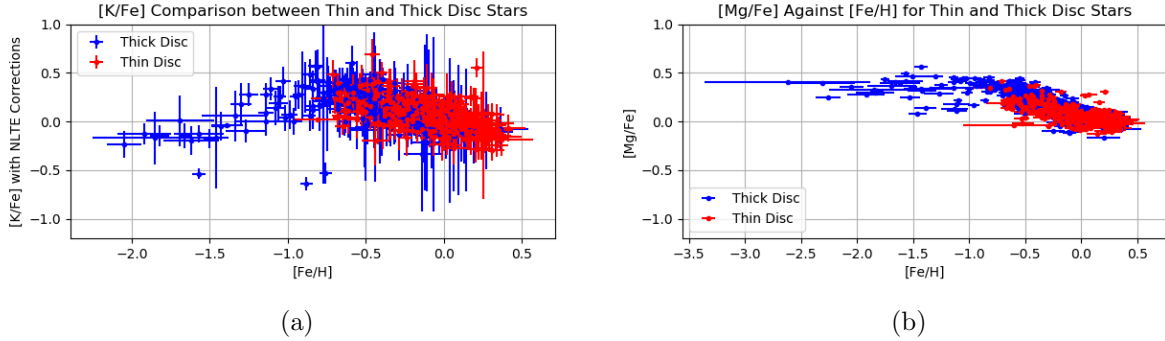


Figure 3.3: (a) NLTE corrected potassium abundance plotted against $[\text{Fe}/\text{H}]$ with a distinction of the thin and the thick discs, (b) $[\text{Mg}/\text{Fe}]$ plotted against $[\text{Fe}/\text{H}]$

Meanwhile, Cayrel et al. (2004) found that the $[\text{K}/\text{Fe}]$ decreases slowly with a decreasing $[\text{Fe}/\text{H}]$ for metal-poor stars with $[\text{Fe}/\text{H}] < -2.5$. This trend would then agree with the presented data here where the $[\text{K}/\text{Fe}]$ tends to decrease for metal-poor stars as the metallicity decreases. In addition, Timmes et al. (1995) predicted decreasing $[\text{K}/\text{Fe}]$ with decreasing $[\text{Fe}/\text{H}]$, while Samland (1998) predicted $[\text{K}/\text{Fe}]$ to remain constant from $[\text{Fe}/\text{H}] = -1.0$ to -3.0 . Therefore, the contradicting predictions and findings indicate the need for the analysis of more data.

Furthermore, the different abundance ratios of $[\text{K}/\text{Fe}]$ for the thin and thick disc stars indicates support to the idea that the discs were created in different spaces and times.

To investigate more into the production of potassium in the thin and thick discs, K was compared to Mg through plots of $[\text{K}/\text{Mg}]$ vs. $[\text{Mg}/\text{H}]$ and $[\text{Fe}/\text{H}]$, shown in figures 3.4(a) and 3.4(b) respectively.

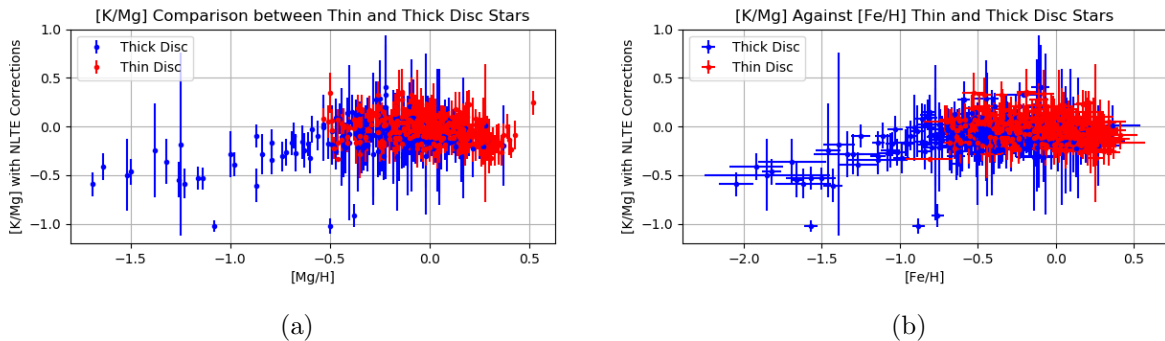


Figure 3.4: (a) $[\text{K}/\text{Mg}]$ plotted against $[\text{Mg}/\text{H}]$, (b) $[\text{K}/\text{Mg}]$ plotted against $[\text{Fe}/\text{H}]$

Since the $[\text{K}/\text{Mg}]$ ratio values do not span a wide range of values, for either $[\text{Mg}/\text{H}]$ or $[\text{Fe}/\text{H}]$, the production of potassium can be said to be connected to the production of α elements Zhang et al. (2006b).

Then K was compared to another α element, Ti. The plots are shown in figures 3.5(a), where $[K/Ti]$ is plotted against $[Ti/H]$, and 3.5(b), where $[K/Ti]$ is plotted against $[Fe/H]$. The trends are similar to those of $[K/Mg]$, where there seems to be a slight increase in $[K/Ti]$ before a flat trend. Again, this points to a connection to the production of α elements.

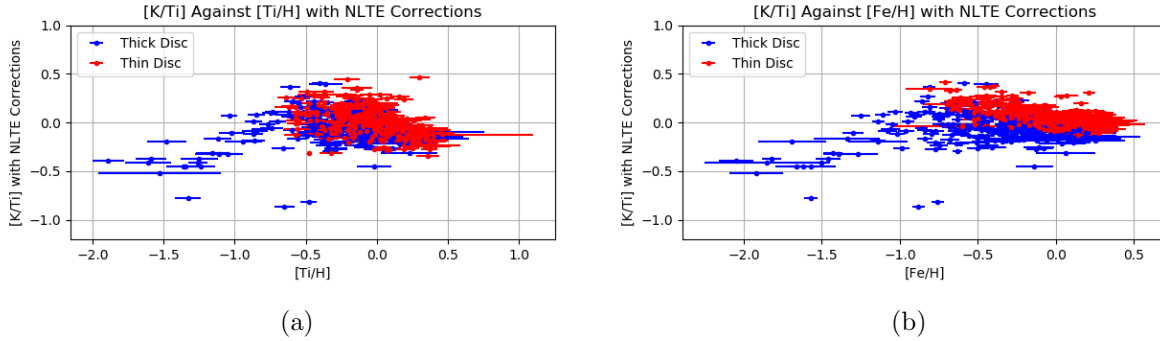


Figure 3.5: (a) $[K/Ti]$ plotted against $[Ti/H]$, (b) $[K/Ti]$ plotted against $[Fe/H]$

Potassium comparison to odd-Z iron peak elements Sc, V, Mn, and Co

The potassium abundances were also compared to odd-Z iron peak elements to explore the links in their production. The data analyzed was collected from Battistini & Bensby (2015) and corresponded to 662 stars, so the identifying HIP numbers were matched to the measured potassium data stars. The resulting plots are shown in figures 3.6(a) to 3.6(d).

The synthesis of Sc is said to originate from neon and carbon burning (Woosley & Weaver 1995), while V, Mn, and Co are said to be created in type II SNe through silicon burning (Woosley & Weaver 1995) as well as through type Ia SNe (Battistini & Bensby 2015).

Elements Sc, V, and Co reveal a flat relation with K, while the $[K/Mn]$ trend seems to increase and then decrease as $[Fe/H]$ increases. This is a similar trend to the $[K/Fe]$ plot, which agrees with the idea that Mn and Fe are created in the same places (Battistini & Bensby 2015). Therefore, it seems as though for lower metallicities, the productions of K dominates over Mn, perhaps through the type II SNe, and as the type Ia SNe occur, the production of Mn begins to dominate, lowering the ratios. Meanwhile, the $[K/X]$ ratios for Sc, V, and Co remain flat, indicating the same amount of each produced during the type II SNe.

Inspecting the plots further reveals the distinctions between the thin and thick disc. For $[K/Sc]$ and $[K/Mn]$ the thick disc stars have a different trend from the thin disc stars at the lower metallicities. $[K/V]$ and $[K/Co]$ show the thin and thick disc stars to have more similar trends.

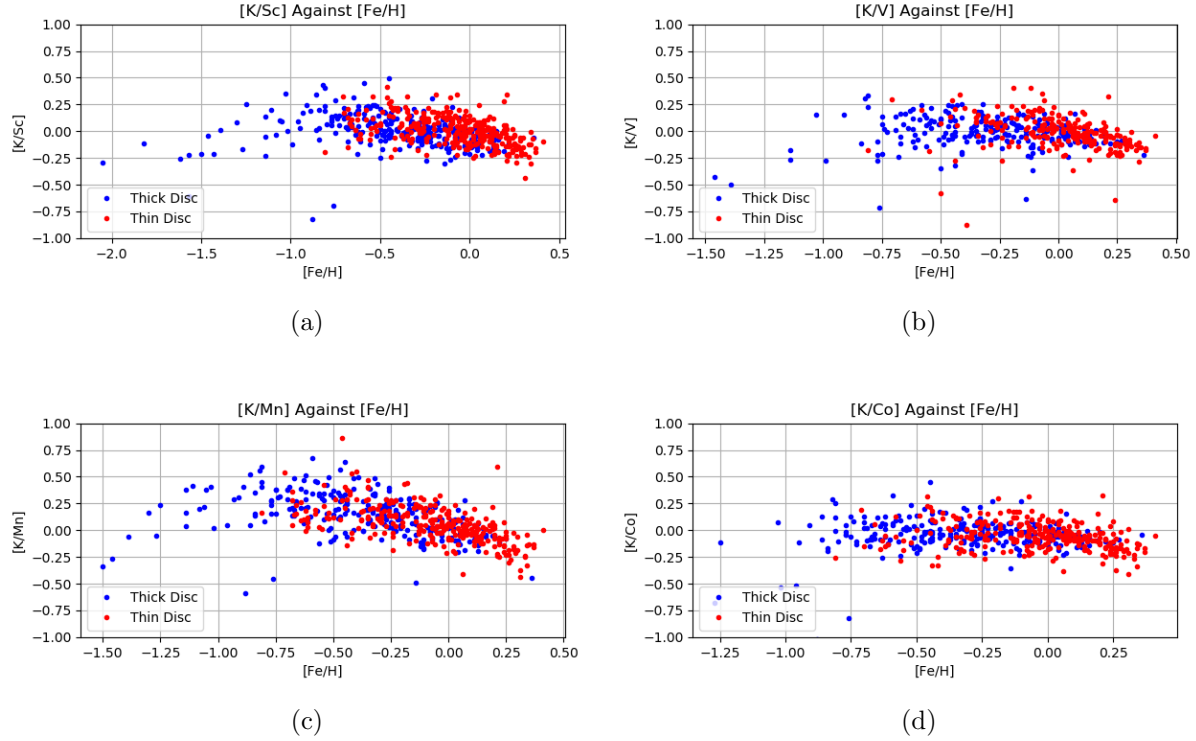


Figure 3.6: (a) $[K/Sc]$ plotted against $[Fe/H]$, (b) $[K/V]$ plotted against $[Fe/H]$, (c) $[K/Mn]$ with NLTE corrections plotted against $[Fe/H]$, (d) $[K/Co]$ with NLTE corrections plotted against $[Fe/H]$

Potassium comparison to r- and s- process elements Sr, Zr, La, Ce, Nd, Sm, Eu

Furthermore, potassium was plotted against the r- and s- process elements of Sr, Zr, La, Ce, Nd, Sm, and Eu. The data on these elements was collected from Battistini & Bensby (2016), which held 593 stars, so again the HIP numbers were matched before analysis. The resulting plots are shown in figures 3.7(a) to 3.7(g).

The r- and s- process is a form of producing the heavy elements. They occur when free neutrons become available for neutron capture, typically from the burning of carbon, oxygen, and silicon (Prialnik 2010). The distinction between the r- and s- processes is whether the capture occurs more rapidly or slowly than the β decays.

Of the elements used here, Eu is an r-process element, La, Sr, Zr, Ce, Sm are s- process elements, and Nd is equally both.

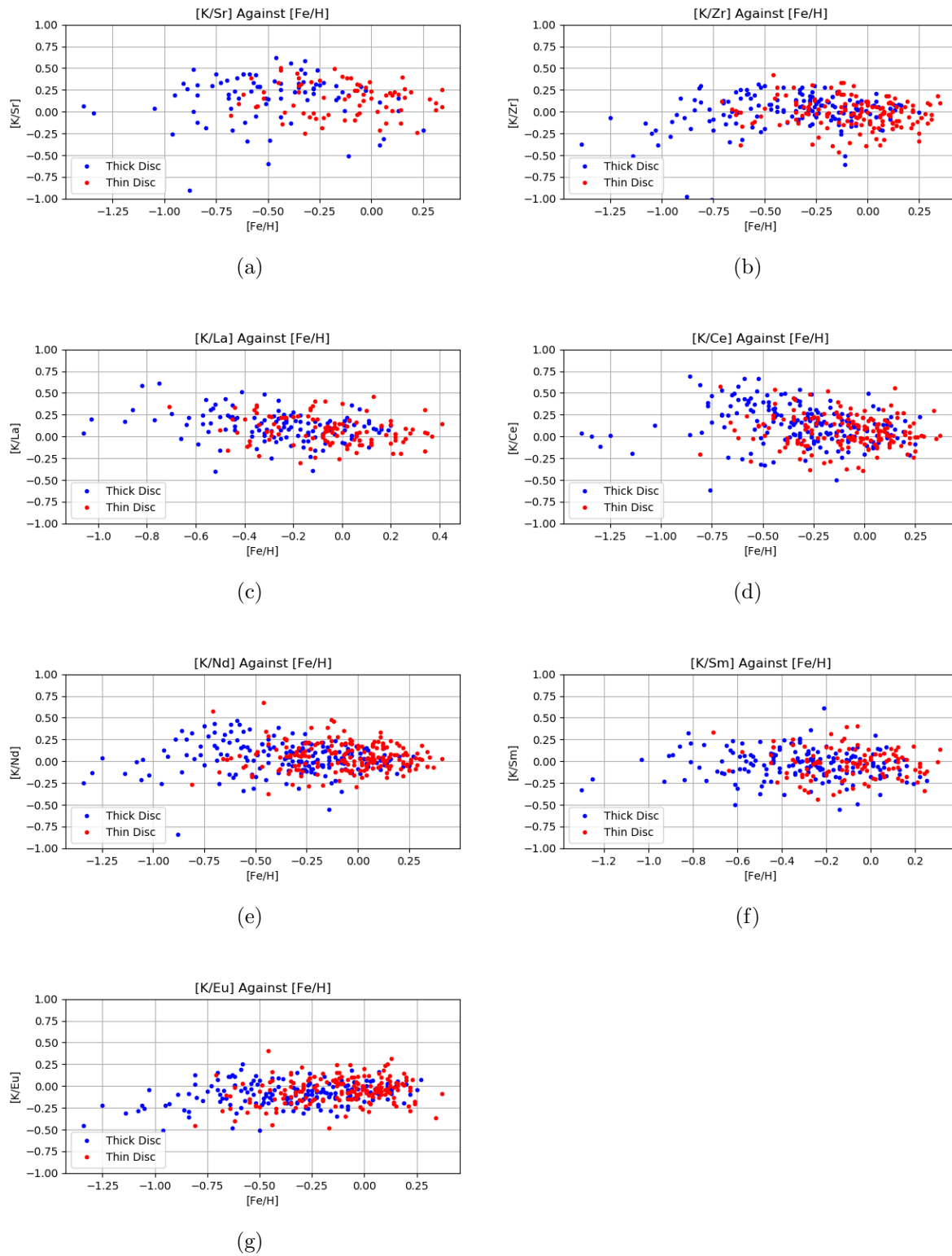


Figure 3.7: [K/Sr], [K/Zr], [K/La], [K/Ce], [K/Nd], [K/Sm], and [K/Eu] plotted against [Fe/H]

Observing these plots, there seems to be uniquely flat trends for each ratio between potassium and the r- and s- process element. This would suggest that they're produced in the same locations. The r- process elements are typically produced as a result of type II SNe activity (Battistini & Bensby 2016), while the s- process elements are created through the burning of He in the core of massive stars and through C burning (Pignatari et al. 2010). R- process element synthesis requires a large amount of neutron flux, which is provided by the core collapse SNe, and follows the path outside the β valley of stability. S- process element synthesis does not require as large neutron flux and follows the β valley of stability. Therefore, the He and C burning produces enough neutrons for the s-process to occur (Battistini & Bensby 2016).

3.3 Discussion

In order to determine accurate potassium abundances, it was appropriate to take into consideration the NLTE effects on the absorption line 7699 Å of potassium, as they had a great influence over the formation of the line. The corresponding corrections were found to have a dependence on temperature, micro-turbulence, and surface gravity, with little dependence on metallicity and absolute K abundance.

Observing the trends with K and the α element Mg, figures 3.4(a) and 3.4(b) ($[K/Mg]$ against $[Mg/H]$ and $[Fe/H]$, respectively), reveal that the ratios do not span a large range of values. This indicates the link between the production of K and Mg in type II SNe. However, there seems to be different trends for the thin and thick disc where the thick disc has an increasing trend for increasing $[Mg/H]$ and $[Fe/H]$. This increasing trend would suggest that some process produces enough K to dominate the ratio, until the production of Mg begins to even out the ratio.

Looking at the trends of $[K/Fe]$ compared to $[Mg/Fe]$ in figures 3.3(a) and 3.3(b), since Mg is an α element, the relation with Fe makes sense according to the production of Mg and Fe in type II SNe and of Fe in type Ia SNe. The production of Mg and Fe remains constant as a ratio during type II SNe events, until type Ia SNe activate and the Fe production dominates, making a decreasing trend. If K were produced in the exact same location as the α elements, it would show the same trend. However it does not, as initially the $[K/Fe]$ increases, and then decreases, indicating a process that dominates with the production of K over Fe, and then the type Ia SNe activate and the Fe production dominates. This matches the trend of $[K/Mg]$ at low $[Mg/H]$ and $[Fe/H]$ and of $[K/Ti]$ at low $[Ti/H]$ and $[Fe/H]$.

These trends with Fe, Mg, and Ti are then repeated with the comparison between K and Mn as an iron peak element. The thick disc stars have an increasing trend before decreasing, which is probably due to the Mn production in type Ia SNe. It is interesting that $[K/Mn]$ and $[K/Fe]$ show the same trends as it is known that Mn and Fe are produced in the same production sites. This confirms the results as then these elements should have the same relation with K.

The r- and s- process elements have flat trends with K, indicating similar production

levels during the different synthesizing events. However, it is strange that there is a flat trend with Eu, as it is mainly produced in type II SNe, and according to the trends with Fe, Mg, and Mn, K is not only produced in type II SNe but also in another process altering the ratios and making K dominate.

Consolidating these trends, it seems as though K can be said to be linked to the production of α elements, as the scatter is low in the [K/Mg] plot, if even with a slight increasing trend at the lower [Mg/H] and [Fe/H] values. In addition, it has a flat trend with Eu, a known type II SNe produce. This agrees with Zhang et al. (2006b) and Zhao et al. (2016). On the other hand, the [K/Fe] ratios point to the idea that the production of K is larger than Fe in the type II SNe, which is unlike the α elements, as they maintain a flat trend.

In the comparison between K and Fe, there are distinct trends between the thin and thick disc stars. This distinction also appears when looking at [K/Mg] and [K/Mn]. The defined thick disc stars in the ratios just mentioned, all have an increasing trend at the lower metallicity values, while the defined thin disc stars either have a decreasing trend or flat trend at the higher metallicity values. As stated previously, this indicates that the thin and thick disc were most likely created in different spaces and times, when observing them through potassium.

3.4 Summary and conclusion

The NLTE corrections are dependent on certain parameters of the star, and this must be taken into consideration to effectively analyze and calculate the potassium abundances.

K does not show typical α element behavior, as there are some non flat trends with [K/Fe] at lower [Fe/H] values, and non flat trends with α elements such as Mg and Ti, which are generated in type II SNe. However, it does have a flat trend with the r- process element Eu, which is also generated in type II SNe. These trends point towards the possibility of a further investigation of K in connection to more r- process elements to see if that uncovers a more clear connection to the production sites. As of now, it seems like K is produced in relatively the same place as α elements, in type II SNe. However, in the ratios of [K/X], where X is Fe, Mg, Ti, and Mn, the K dominates in the more negative, respective, [X/H] and [Fe/H] regions.

In the plots of [K/Mg] and [K/Fe] and [K/Ti], figures 3.3(a), 3.4(a), 3.4(b), 3.5(a), 3.5(b), distinct trends between the thin and thick disc stars are visible. The thin disc stars tend to have little spread in the [K/X] ratios, and have either a flat or decreasing trend with increasing [X/H] and [Fe/H]. Meanwhile, the thick disc stars have a larger spread in the [K/X] ratios, and have an increasing trend from the lower [X/H] and [Fe/H] regions. This points to the idea that the thin and thick disc stars have different evolutionary patterns when it comes to K.

In terms of the analysis of the thin and thick disc stars in relation to K, this project analyzed the largest sample of data with K abundances. This is useful because there is a view into the trends at lower metallicities, [Fe/H] \leq - 1.5, as well as around and above the

solar metallicity.

To improve the method and results, as well as deepen the understanding of the role of K in uncovering the chemical evolution of the galaxy, there are several steps that could be altered. The first is in the way of measuring the EWs, since it was done by hand, human error most likely skewed the placements of the fits each time the absorption peaks were fitted. A more precise method of measuring the EWs would be useful for more precise abundance calculations. Then, in the interpolation of the stellar parameters with the tables of NLTE corrections, simple linear relationships were assumed both for interpolation and extrapolation. To ensure that the resulting NLTE corrections calculated for the stars were more accurate, either a larger sample of NLTE corrections with larger variations of the temperature, K abundance, $\log g$, micro-turbulence, and $[\text{Fe}/\text{H}]$ could be used, or a deeper study of the relationship between the NLTE corrections and the stellar parameters could be conducted. In addition, the analysis in this project revealed some connection to the production site of K and α elements, as well to as to other elements also produced in type II SNe like Eu and Co. To further the understanding of the production of K in relation to iron peak elements and r- and s- process elements, more element ratios of these types could be calculated and explored. Moreover, the connection between K and r-process elements seems like an interesting lead to follow, as in the $[\text{K}/\text{Eu}]$ plot there is little scatter and a flat trend for both the thin and thick disc, meaning that there is a connection to their production sites.

While the results confirm the distinction of K abundance trends in the thin and thick discs, they do not clearly indicate a reason or explanation of the different evolutions of the two discs. Knowing the production sites of K in the two discs as well as that there are distinct trends, adds to the present research and knowledge of how the two discs evolved. With additional data and comparisons of K to other elements and relations to their production sites, a clearer view into the differing evolutionary history of the Milky Way galaxy can be achieved.

Bibliography

- Adelman, S. J., Gulliver, A. F., & Holmgren, D. E. 1996, in *Astronomical Society of the Pacific Conference Series*, Vol. 108, M.A.S.S., *Model Atmospheres and Spectrum Synthesis*, ed. S. J. Adelman, F. Kupka, & W. W. Weiss, 293
- Barklem, P. S. & Aspelund-Johansson, J. 2005, *Astron. and Astrophys.*, 435, 373, (BA-J)
- Barklem, P. S., Piskunov, N., & O'Mara, B. J. 2000, *Astron. and Astrophys. Suppl. Ser.*, 142, 467, (BPM)
- Battistini, C. & Bensby, T. 2015, *A&A*, 577, A9
- Battistini, C. & Bensby, T. 2016, *A&A*, 586, A49
- Bensby, T., Feltzing, S., & Oey, M. S. 2014, *A&A*, 562, A71
- Cayrel, R., Depagne, E., Spite, M., et al. 2004, *A&A*, 416, 1117
- Epstein, C. R., Johnson, J. A., Dong, S., et al. 2010, *ApJ*, 709, 447
- Fuhr, J. R., Martin, G. A., & Wiese, W. L. 1988, *Journal of Physical and Chemical Reference Data*, Volume 17, Suppl. 4. New York: American Institute of Physics (AIP) and American Chemical Society, 1988, 17, (FMW)
- Gilmore, G. & Reid, N. 1983, *MNRAS*, 202, 1025
- Gray, D. F. 2005, *The Observation and Analysis of Stellar Photospheres* (Cambridge University Press)
- Kubát, J. 2014, *Basics of the NLTE Physics*, ed. E. Niemczura, B. Smalley, & W. Pych, 149–157
- Kurucz, R. L. 2004, Robert L. Kurucz on-line database of observed and predicted atomic transitions
- Kurucz, R. L. 2007, Robert L. Kurucz on-line database of observed and predicted atomic transitions

- Kurucz, R. L. 2008, Robert L. Kurucz on-line database of observed and predicted atomic transitions
- Kurucz, R. L. 2010, Robert L. Kurucz on-line database of observed and predicted atomic transitions
- Kurucz, R. L. 2012, Robert L. Kurucz on-line database of observed and predicted atomic transitions
- Kurucz, R. L. 2013, Robert L. Kurucz on-line database of observed and predicted atomic transitions
- Kurucz, R. L. 2014, Robert L. Kurucz on-line database of observed and predicted atomic transitions
- Matteucci, F. 2016, in Journal of Physics Conference Series, Vol. 703, Journal of Physics Conference Series, 012004
- Minchev, I., Famaey, B., Quillen, A. C., et al. 2012, *A&A*, 548, A127
- Mushotzky, R. 2015, University of Maryland
- O'Brian, T. R., Wickliffe, M. E., Lawler, J. E., Whaling, W., & Brault, J. W. 1991, Journal of the Optical Society of America B Optical Physics, 8, 1185, (BWL)
- Pignatari, M., Gallino, R., Heil, M., et al. 2010, *ApJ*, 710, 1557
- Prialnik, D. 2010, *An Introduction to the Theory of Stellar Structure and Evolution* (Cambridge University Press)
- Raassen, A. J. J. & Uylings, P. H. M. 1998, *A&A*, 340, 300, (RU)
- Ralchenko, Y., Kramida, A., Reader, J., & NIST ASD Team. 2010, NIST Atomic Spectra Database (ver. 4.0.0), [Online].
- Samland, M. 1998, *ApJ*, 496, 155
- Shimansky, V. V., Bikmaev, I. F., Galeev, A. I., et al. 2003, *Astronomy Reports*, 47, 750
- Takeda, Y., Zhao, G., Chen, Y.-Q., Qiu, H.-M., & Takada-Hidai, M. 2002, *PASJ*, 54, 275
- Timmes, F. X., Woosley, S. E., & Weaver, T. A. 1995, *ApJS*, 98, 617
- Woosley, S. E. & Weaver, T. A. 1995, *APJS*, 101, 181
- Zhang, H. W., Butler, K., Gehren, T., Shi, J. R., & Zhao, G. 2006a, *A&A*, 453, 723
- Zhang, H. W., Gehren, T., Butler, K., Shi, J. R., & Zhao, G. 2006b, *A&A*, 457, 645
- Zhao, G., Mashonkina, L., Yan, H. L., et al. 2016, *ApJ*, 833, 225

Appendix A

NLTE K abundances and corrections

Table A.1: Table of the final K abundances and their NLTE corrections

HIP	NLTE K	NLTE Correction
80	-0.268020413	-0.447135465
305	0.142937336	-0.416177717
407	0.058571058	-0.310543995
699	-0.037112493	-0.536227545
768	-0.00510327	-0.444218322
910	-0.13126514	-0.540380192
950	0.117020504	-0.532094549
1128	-0.534205853	-0.453320905
1349	-0.275724565	-0.404839618
1599	0.195033486	-0.454081566
1746	-0.375372346	-0.344487399
1877	-0.057500526	-0.196615578
1931	0.093427091	-0.515687961
1955	0.029798173	-0.44931688
1976	0.14029369	-0.428821362
2021	0.080840269	-0.398274784
2057	0.002986308	-0.236128745
2194	-0.474723724	-0.243838776
2235	-0.16742193	-0.606536982
2319	-0.344483376	-0.603598428
2711	0.094379123	-0.58473593
2743	-0.306778438	-0.15589349
2787	0.140411013	-0.578704039
2909	0.00573605	-0.353379003
3026	nan	-0.713282358
3086	-0.071686322	-0.410801374
3142	-0.31830112	-0.607416173

APPENDIX A. NLTE K ABUNDANCES AND CORRECTIONS

HIP	NLTE K	NLTE Correction
3170	-0.267092271	-0.596207324
3182	-0.18606666	-0.355181712
3185	-0.300082265	-0.289197318
3391	0.131227928	-0.277887124
3479	-0.247201641	-0.366316694
3497	-0.257972195	-0.347087247
3704	-0.351448012	-0.510563065
3734	0.144642012	-0.48447304
3909	0.068564519	-0.510550534
4830	0.143439948	-0.465675104
4892	-0.217118722	-0.476233775
5054	-0.42359476	-0.572709812
5264	0.132519415	-0.376595638
5301	-0.25937646	-0.458491512
5315	nan	-0.189536642
5700	0.006348895	-0.362766158
5817	-0.152878573	-0.211993626
5862	nan	-0.551814732
6177	-0.019390976	-0.148506028
6607	-0.29371977	-0.322834822
6653	0.180621425	-0.358493627
6856	0.182828056	-0.176286997
6949	-0.213779249	-0.192894301
7080	0.260924734	-0.318190319
7091	-0.0387001	-0.207815153
7162	-2.284384942	-0.663499995
7276	0.214725272	-0.404389781
7961	-0.193745489	-0.392860541
7978	0.073093463	-0.446021589
8398	0.184904736	-0.384210317
8498	-0.069121431	-0.428236484
8572	nan	-0.437637631
8674	-0.45577985	-0.374894902
8758	0.002392984	-0.406722068
8798	-0.130885295	-0.400000348
8859	-0.20920625	-0.578321302
9085	nan	-0.47917439
9137	-0.278407326	-0.657522378
9316	0.277507196	-0.311607856
9381	-0.151401042	-0.360516094
9471	0.160065772	-0.36904928
9629	-0.205738585	-0.254853637

APPENDIX A. NLTE K ABUNDANCES AND CORRECTIONS

HIP	NLTE K	NLTE Correction
9818	0.127768126	-0.301346927
9911	0.075370898	-0.413744155
10116	0.122402055	-0.386712998
10225	0.197845587	-0.631269466
10306	0.219843683	-0.549271369
10483	-0.096807656	-0.495922709
10492	0.320693652	-0.318421401
10694	0.108575629	-0.360539423
10798	-0.599781542	-0.258896594
10842	-0.26125878	-0.330373833
10977	-0.474175975	-0.143291027
11072	0.048804548	-0.460310504
11205	-0.074157822	-0.233272875
11309	-0.141023052	-0.540138105
11586	-0.055430135	-0.564545187
12048	0.122093685	-0.337021368
12186	0.163180655	-0.335934397
12306	nan	-0.530464139
12381	-0.101765471	-0.540880523
12411	-0.1743325	-0.313447553
12444	0.073211215	-0.525903837
12483	-0.308485125	-0.407600177
12611	0.285604645	-0.243510408
12653	0.137728519	-0.521386533
12889	-0.124340773	-0.503455825
13315	-0.336152125	-0.575267178
13341	-0.134522609	-0.503637661
13350	-0.189922527	-0.279037579
13366	-0.427998749	-0.557113802
13388	-0.287627932	-0.196742985
13513	-0.087519158	-0.17663421
13848	0.097578046	-0.211537006
13902	-0.171206455	-0.490321507
13938	0.107630937	-0.511484116
14016	0.005495034	-0.273620019
14023	0.054007114	-0.165107938
14086	-0.265306236	-0.274421288
14241	-0.205672989	-0.284788042
14339	-0.172035232	-0.491150284
14561	0.17579877	-0.483316283
14879	-0.079650116	-0.578765169
14954	0.015914542	-0.553200511

APPENDIX A. NLTE K ABUNDANCES AND CORRECTIONS

HIP	NLTE K	NLTE Correction
15131	nan	-0.471754575
15158	-0.051910544	-0.561025596
15371	-0.28122033	-0.470335382
15381	0.083076348	-0.406038704
15510	nan	-0.273436635
15940	-0.217991086	-0.407106138
16169	-0.366801268	-0.40591632
16365	-0.133048233	-0.392163286
16391	0.100969471	-0.328145582
16404	nan	-0.472335331
16492	-0.30351562	-0.192630672
16788	-0.291424418	-0.54053947
16852	-0.08836285	-0.597477902
17147	-0.791090969	-0.550206022
17378	0.183228598	-0.175886455
17970	-0.509357123	-0.228472175
17987	-0.15028259	-0.349397643
18164	-0.421645514	-0.680760567
18331	0.166581854	-0.552533199
18612	-0.078589034	-0.437704086
18802	-0.653686809	-0.482801861
18833	-0.155334559	-0.594449611
19233	-0.073962024	-0.453077077
19773	-0.313739199	-0.602854252
20199	-0.174956239	-0.354071292
20242	0.110685304	-0.358429748
20489	0.193459742	-0.335655311
20638	-0.172746567	-0.371861619
20677	-0.078642092	-0.357757145
21079	-0.13938496	-0.438500012
21731	0.112488178	-0.306626875
21832	-0.393666446	-0.392781498
21839	0.063680222	-0.38543483
22068	nan	-0.65883407
22162	0.055531767	-0.423583285
22263	-0.076482521	-0.375597574
22278	0.026406556	-0.352708497
22325	0.29725608	-0.491858973
22336	0.126492506	-0.432622546
22349	-0.159550964	-0.388666017
22395	0.056639058	-0.412475994
22632	-1.816953663	-0.656068715

APPENDIX A. NLTE K ABUNDANCES AND CORRECTIONS

HIP	NLTE K	NLTE Correction
22824	-0.001992668	-0.47110772
23383	-0.16991519	-0.259030243
23555	0.101830026	-0.527285026
23941	0.039860823	-0.529254229
24037	-0.299923222	-0.289038274
24682	-0.133997272	-0.243112325
24722	-0.121663303	-0.310778355
24819	0.10388149	-0.145233562
24829	nan	-0.497752235
25209	0.201050217	-0.648064835
25528	0.100213233	-0.65890182
25905	-0.24556191	-0.294676963
26273	-0.199422188	-0.328537241
26641	nan	-0.30869592
26828	0.021034813	-0.54808024
27072	nan	-0.523751273
27080	-0.481855557	-0.220970609
27128	-1.521593571	-0.560708623
27910	0.003828185	-0.155286867
28044	0.204491617	-0.244623436
28066	0.045849578	-0.343265475
28159	nan	-0.421990002
28267	-0.074775497	-0.263890549
28369	0.112296651	-0.626818401
28403	-0.230997953	-0.340113006
28671	nan	-0.350224859
29271	-0.008244774	-0.267359827
29716	0.088417541	-0.600697512
30158	0.047815487	-0.331299565
30439	-0.209525793	-0.308640846
30476	0.1229153	-0.306199752
30480	0.122295711	-0.446819342
30503	-0.0691524	-0.428267453
30545	0.040166357	-0.468948695
31030	-0.173244259	-0.232359311
32649	0.016709343	-0.26240571
33094	0.050819159	-0.458295893
33220	-0.340860637	-0.59997569
33324	-0.503881736	-0.492996789
33582	-0.290892209	-0.540007261
33642	-0.043189933	-0.442304986
34017	nan	-0.433459932

APPENDIX A. NLTE K ABUNDANCES AND CORRECTIONS

HIP	NLTE K	NLTE Correction
34028	0.234603346	-0.234511706
34065	-0.166497079	-0.415612131
34069	-0.240940769	-0.190055821
34212	-0.088937183	-0.648052236
34254	0.068538253	-0.310576799
34285	-0.956760374	-0.555875427
34410	-0.06874885	-0.547863902
34511	-0.077027828	-0.386142881
34739	-0.263232014	-0.282347066
34961	-0.236398022	-0.235513074
35139	-0.494344576	-0.453459629
35148	-0.198518049	-0.497633101
35318	-0.17401639	-0.483131442
35718	0.003755699	-0.235359353
35750	-0.053226972	-0.112342024
36210	-0.063366038	-0.292481091
36269	-1.806782762	-0.595897815
36491	-0.688321596	-0.677436649
36515	-0.143766137	-0.48288119
36795	nan	-0.588061859
36849	-0.507542424	-0.556657477
36855	nan	-0.319715372
36874	-0.046171913	-0.385286965
36993	nan	-0.387788064
37171	0.058021732	-0.29109332
37233	-0.057958978	-0.407074031
37419	-0.140851434	-0.329966487
37520	nan	-0.369499985
37789	-0.411521852	-0.490636905
37853	-0.408041056	-0.477156109
38134	-0.539013709	-0.488128762
38541	nan	-0.498230071
38625	-0.54263023	-0.261745282
38750	-0.045261345	-0.494376398
38782	-0.025439073	-0.414554126
38862	-0.213787414	-0.412902467
38926	nan	-0.601512227
39911	-0.677535229	-0.426650281
40613	-0.405469342	-0.604584395
40761	nan	-0.442799123
40794	-0.088379767	-0.45749482
41471	-0.04579339	-0.524908442

APPENDIX A. NLTE K ABUNDANCES AND CORRECTIONS

HIP	NLTE K	NLTE Correction
41544	nan	-0.648189144
42356	nan	-0.42972665
42612	-0.012307322	-0.401422374
42734	nan	-0.479418724
42889	-0.138762439	-0.417877492
43054	-0.022701241	-0.481816294
43393	-0.520396276	-0.309511329
44075	nan	-0.743625123
44319	0.112107656	-0.407007397
44441	nan	-0.551905617
44713	0.089361687	-0.399753366
44821	-0.082906545	-0.122021598
44860	-0.255572009	-0.404687062
44896	-0.123046322	-0.482161374
44915	0.100598048	-0.578517004
44927	0.1728351	-0.506279952
45283	-0.629722113	-0.568837166
45514	-0.032559116	-0.231674168
45733	-0.429887792	-0.579002845
46685	0.07275669	-0.206358363
46888	0.034743224	-0.394371829
47048	-0.396284893	-0.625399946
47588	-0.226547292	-0.495662344
48152	-2.050742228	-0.56985728
48468	0.219784152	-0.4593309
49285	-0.063348298	-0.292463351
49793	nan	-0.460212785
49942	nan	-0.438853866
49988	-0.159337744	-0.468452796
50274	-0.302685828	-0.211800881
50316	-0.181561907	-0.460676959
50671	-0.273627129	-0.472742181
50713	-0.326750501	-0.275865554
50834	-0.316399818	-0.595514871
50907	0.160608643	-0.568506409
50941	-0.229045654	-0.318160707
51028	-0.387774365	-0.566889418
51078	0.280133986	-0.368981067
51477	nan	-0.454502369
51579	-0.08757935	-0.466694403
51614	0.175569724	-0.463545329
51933	-0.104839525	-0.563954577

APPENDIX A. NLTE K ABUNDANCES AND CORRECTIONS

HIP	NLTE K	NLTE Correction
51938	-0.074639344	-0.383754397
52247	-0.077244787	-0.25635984
52325	-0.05846673	-0.407581783
52564	0.034142102	-0.164972951
52990	0.09954081	-0.399574242
53122	-0.08178185	-0.380896903
53311	nan	-0.49540792
53719	-9.44E-05	-0.119209431
53765	-0.27702838	-0.556143433
53982	0.1437095	-0.445405553
54043	-0.250920885	-0.360035938
54469	-0.14744091	-0.476555962
54641	-1.136764674	-0.625879727
54779	-0.370916862	-0.540031914
54924	-0.639776854	-0.538891906
55210	nan	-0.248638728
55278	0.015536631	-0.603578421
55592	-0.983846276	-0.602961329
55805	-0.876621986	-0.445737039
56004	0.146649631	-0.452465422
56336	-0.450196013	-0.489311065
56389	-0.114394196	-0.423509249
56452	-0.34014397	-0.199259022
56557	0.010674885	-0.268440168
56664	-0.624251281	-0.673366334
56830	-0.250062753	-0.239177805
56845	-0.130823139	-0.229938192
56868	-0.150262541	-0.379377594
57017	nan	-0.618102793
57216	-0.271116191	-0.550231244
57360	-1.370505994	-0.609621047
58145	-1.049602261	-0.628717314
58153	nan	-0.30130021
58401	-0.54616047	-0.205275522
58517	0.014357378	-0.504757675
58576	nan	-0.221409324
58843	-0.725315787	-0.58443084
58950	nan	-0.411064772
58962	-0.801996166	-0.521111219
59021	0.058756026	-0.460359027
59380	nan	-0.481913685
59490	-1.476068559	-0.555183611

APPENDIX A. NLTE K ABUNDANCES AND CORRECTIONS

HIP	NLTE K	NLTE Correction
59532	nan	-0.236372599
59639	-0.097685359	-0.146800411
59696	-0.376111486	-0.225226539
59699	-0.422336124	-0.561451176
60019	nan	-0.537588405
60288	0.114629429	-0.494485624
60462	-0.560430067	-0.21954512
60574	-0.06200117	-0.291116222
60632	nan	-0.513810892
60729	0.086853471	-0.382261582
60825	-0.573876514	-0.562991567
60956	nan	-0.290625802
61619	0.187777806	-0.511337247
61802	-0.971045924	-0.410160976
61971	-0.284243699	-0.303358751
62108	nan	-0.631587381
62534	-0.322098801	-0.311213854
62607	-0.422332179	-0.271447231
62809	nan	-0.394061073
62857	-0.01441112	-0.483526172
63405	-0.179474727	-0.65858978
63548	nan	-0.300239486
63918	-0.256360526	-0.495475579
64345	nan	-0.444595505
64408	nan	-0.306959928
64426	-0.408549845	-0.517664897
64444	-0.003708284	-0.472823337
64459	nan	-0.498864541
64673	0.109006278	-0.400108774
64698	-0.181325657	-0.42044071
64706	-0.235420775	-0.134535827
64747	nan	-0.367853775
64792	0.26415322	-0.454961833
64920	nan	-0.169716327
64924	-0.158155288	-0.327270341
66238	-0.135543135	-0.304658188
66814	nan	-0.233861376
67371	0.389362241	-0.359752811
67534	nan	-0.620844076
67784	-0.040927699	-0.570042751
67863	-1.293572825	-0.402687877
68273	-0.250078503	-0.269193556

APPENDIX A. NLTE K ABUNDANCES AND CORRECTIONS

HIP	NLTE K	NLTE Correction
68464	-1.967372681	-0.536487734
68468	0.026613054	-0.432501998
68727	-0.459671561	-0.668786613
68796	nan	-0.480990388
69220	-0.239133955	-0.368249008
69645	-0.126884672	-0.465999725
69780	-0.253814129	-0.472929181
69796	-0.065997387	-0.495112439
70140	-0.22049392	-0.419608973
70182	0.008289329	-0.490825724
70330	0.133718803	-0.39539625
70681	-1.126325471	-0.425440524
70829	-0.443532745	-0.322647798
70922	-0.457510702	-0.466625755
71019	-0.040005792	-0.259120844
71284	-0.215915415	-0.695030468
71470	-0.581182569	-0.730297621
71735	-0.291162883	-0.320277935
71844	-0.446694577	-0.58580963
72479	nan	-0.144509321
72673	-0.540610222	-0.639725274
72688	-0.021182432	-0.120297485
72797	nan	-0.233996456
73385	nan	-0.501116573
73444	nan	-0.633525609
73650	-0.036475212	-0.505590264
74033	nan	-0.532700565
74067	nan	-0.642752426
74079	-0.243100978	-0.48221603
74234	-1.433155787	-0.29227084
74235	-1.627358229	-0.336473282
74389	0.062432829	-0.366682223
74500	0.081772286	-0.427342766
74537	-0.082787965	-0.191903017
74831	-0.237803836	-0.446918889
75023	0.234294323	-0.57482073
75181	-0.286158964	-0.365274016
75206	0.431264536	-0.527850516
75487	-0.443678984	-0.542794037
76226	-0.517211057	-0.676326109
76394	-0.103291613	-0.472406665
76899	nan	-0.426277704

APPENDIX A. NLTE K ABUNDANCES AND CORRECTIONS

HIP	NLTE K	NLTE Correction
76976	nan	-0.423178947
76984	0.091649867	-0.357465186
77358	0.060132797	-0.308982255
77439	-0.315601351	-0.604716404
77536	0.195997806	-0.703117247
77637	nan	-0.547318451
77641	0.144979783	-0.254135269
78267	nan	-0.418144727
78330	-0.207116239	-0.426231292
78425	0.012939656	-0.376175396
78551	-0.106823015	-0.265938068
78556	-0.085700869	-0.394815922
78640	nan	-0.63241096
78917	-0.619177166	-0.328292218
78955	0.214563453	-0.354551599
79073	0.142923066	-0.396191987
79137	0.213033766	-0.106081287
79138	-0.27217545	-0.551290503
79576	-0.526519738	-0.33563479
79715	-0.162470635	-0.461585687
79792	-0.078826298	-0.417941351
80013	0.033409436	-0.355705616
80043	-0.363797829	-0.152912881
80114	nan	-0.438928047
80221	-0.550807207	-0.33992226
80337	-0.031779637	-0.42089469
80423	nan	-0.695403015
80587	-0.354971703	-0.484086756
80686	-0.243847083	-0.622962136
80700	-0.082315866	-0.261430919
80722	-0.140227617	-0.549342669
80837	nan	-0.641630245
81041	-0.228653058	-0.457768111
81269	0.064808363	-0.404306689
81300	-0.081786577	-0.220901629
81461	-0.386512896	-0.555627949
81520	-0.632859406	-0.551974458
81580	-0.412242201	-0.581357253
81603	-0.004591885	-0.333706938
81749	0.072308497	-0.246806556
81952	0.309895041	-0.329220011
82062	-0.446356222	-0.585471275

APPENDIX A. NLTE K ABUNDANCES AND CORRECTIONS

HIP	NLTE K	NLTE Correction
82265	0.172605714	-0.206509338
82588	-0.185042196	-0.274157248
82621	0.252868953	-0.3362461
83204	-0.212526909	-0.491641962
83229	-0.362089044	-0.471204097
83241	-0.233895443	-0.523010495
83276	-0.053688458	-0.452803511
83301	0.068303586	-0.620811466
83489	-0.1572147	-0.426329753
83562	-0.226413239	-0.415528292
83601	0.110156643	-0.488958409
83867	-0.038768641	-0.507883694
84255	-0.629209515	-0.368324568
84551	nan	-0.537365356
84636	0.222755806	-0.496359247
84781	-0.072025694	-0.291140747
84803	0.040822385	-0.428292667
84905	nan	-0.500068828
84907	-0.082546892	-0.211661944
84988	-0.372191701	-0.411306754
85007	-0.433519096	-0.522634149
85042	-0.158261185	-0.337376238
85320	0.075364616	-0.163750437
85474	0.762129949	-0.486985103
85757	nan	-0.396272558
85963	-0.408897645	-0.648012698
85969	0.046340774	-0.422774278
86013	-0.3816187	-0.500733752
86193	0.049829607	-0.319285446
86516	-0.074838593	-0.383953645
86694	-2.021032217	-0.55014727
86731	0.180112646	-0.439002406
86796	nan	-0.312340954
87101	-2.106985363	-0.596100416
87154	0.143258381	-0.285856671
87443	0.13336111	-0.355753943
87523	-0.203595844	-0.522710897
87533	0.118355986	-0.500759066
87539	-0.371684272	-0.520799325
87679	0.090562535	-0.208552518
87769	0.129866233	-0.31924882
87841	0.06722205	-0.421893003

APPENDIX A. NLTE K ABUNDANCES AND CORRECTIONS

HIP	NLTE K	NLTE Correction
88010	-1.285107473	-0.444222525
88622	nan	-0.439296046
88631	0.286215841	-0.292899212
88945	0.143009462	-0.40610559
89036	-0.038689576	-0.477804628
89076	0.032881547	-0.336233506
89105	0.0906649	-0.318450153
89207	0.056548895	-0.382566157
89554	-1.694491141	-0.533606194
89583	-0.229371615	-0.288486668
89589	-0.077852823	-0.506967875
89733	-0.14636319	-0.395478243
89881	0.132035092	-0.27707996
89952	-0.320527314	-0.619642367
90004	-0.04195942	-0.281074473
90151	0.173683712	-0.15543134
90261	-0.921631454	-0.560746507
90365	-0.231839251	-0.250954303
90442	-0.245109979	-0.464225031
90485	0.427897608	-0.491217444
90539	-0.175529932	-0.214644985
90896	0.170793405	-0.318321648
91089	-0.13675557	-0.535870623
91095	-0.221239081	-0.500354133
91360	nan	-0.170314588
91438	-0.428110377	-0.417225429
91471	0.003247768	-0.135867284
91582	0.027036737	-0.252078316
92270	-0.085346184	-0.574461237
92288	-0.203722001	-0.592837053
92781	-0.372918551	-0.422033604
92864	0.116327727	-0.522787325
92880	-0.006889301	-0.466004353
92973	-0.257022543	-0.486137595
93185	-0.386886857	-0.49600191
93186	nan	-0.475453616
93377	-0.116845977	-0.38596103
93507	-0.491385103	-0.690500156
93889	0.039384531	-0.419730522
93966	0.140772268	-0.308342785
94347	-0.430372451	-0.589487503
94645	0.078967626	-0.540147427

APPENDIX A. NLTE K ABUNDANCES AND CORRECTIONS

HIP	NLTE K	NLTE Correction
94678	-0.083754927	-0.492869979
95106	-0.27444429	-0.403559343
95262	-0.24082276	-0.509937813
95447	0.344278957	-0.264836096
96124	-0.131907985	-0.321023037
96160	-0.035541579	-0.384656632
96258	-0.077772399	-0.606887452
96425	-0.001293162	-0.240408214
96536	0.125221517	-0.583893535
96854	-3.06E-05	-0.319145651
96881	-0.214616297	-0.503731349
97024	-0.063180735	-0.322295787
97213	0.160600302	-0.39851475
97358	-0.033713223	-0.282828276
97676	0.050639113	-0.33847594
97779	0.057078611	-0.462036441
98020	-1.681323313	-0.440438365
98355	nan	-0.6900158
98416	-0.031405235	-0.400520287
98532	-0.861075931	-0.590190984
98565	-0.162547577	-0.65166263
98767	0.170211045	-0.318904008
98785	0.307685445	-0.461429608
98964	0.051167335	-0.217947718
99100	-0.141668903	-0.420783955
99139	-0.19862759	-0.347742643
99174	0.069227455	-0.409887597
99224	nan	-0.293020566
99240	0.178834442	-0.29028061
99551	-0.127604396	-0.476719449
99799	-0.146436477	-0.455551529
100394	-0.283978617	-0.60309367
100405	-0.342561938	-0.301676991
100412	-0.182679988	-0.56179504
100568	nan	-0.508922455
100792	nan	-0.601762623
100942	0.169405941	-0.349709111
100970	0.091393897	-0.427721156
101346	-0.342766251	-0.591881303
101399	0.056910529	-0.362204524
101857	-0.001405236	-0.330520289
102018	0.221932216	-0.407182837

APPENDIX A. NLTE K ABUNDANCES AND CORRECTIONS

HIP	NLTE K	NLTE Correction
102046	-0.790527245	-0.569642298
102200	-0.404541257	-0.43365631
102264	-0.331300293	-0.330415345
102548	-0.213547238	-0.30266229
102580	0.066129274	-0.252985778
102610	-0.176134115	-0.415249167
102762	-0.04144809	-0.460563143
102793	nan	-0.460864096
102838	-0.11200453	-0.421119583
103458	-0.503718655	-0.502833707
103498	-0.774012693	-0.543127745
103572	-0.432598761	-0.501713813
103609	0.00381839	-0.185296663
103654	0.042603826	-0.516511227
103682	0.165636566	-0.383478486
103692	0.085829359	-0.423285693
103735	-0.032430945	-0.351545998
103773	-0.15320119	-0.422316243
103881	-0.351494782	-0.590609835
103896	-0.40862949	-0.557744543
103990	0.313249638	-0.405865414
104045	-0.060792539	-0.439907592
104075	0.034200499	-0.454914554
104152	0.134222701	-0.424892352
104294	-0.138061687	-0.567176739
104560	-0.389101884	-0.418216936
104659	-0.941244797	-0.60035985
104672	0.064732706	-0.474382347
104766	-0.02577352	-0.564888572
104922	0.042212824	-0.336902229
105083	0.082319082	-0.556795971
105214	0.071183912	-0.427931141
105521	0.164615795	-0.414499258
105541	0.014133183	-0.35498187
105606	0.234658712	-0.284456341
105790	-0.140005635	-0.279120688
105858	-0.527983204	-0.547098256
106006	0.014968121	-0.434146932
106560	-0.424778832	-0.413893884
106678	0.024994066	-0.344120987
106701	0.090608552	-0.318506501
106931	-0.118422282	-0.247537334

APPENDIX A. NLTE K ABUNDANCES AND CORRECTIONS

HIP	NLTE K	NLTE Correction
106951	-0.023926429	-0.353041481
107607	-0.474044418	-0.50315947
107618	-0.21784377	-0.376958822
107708	-0.215340587	-0.414455639
107857	-0.341705731	-0.280820783
107877	-0.11536408	-0.574479132
107975	-0.310691336	-0.529806388
108068	-0.280647961	-0.409763014
108095	-0.432263899	-0.611378951
108158	0.026200436	-0.302914616
108288	-0.196854335	-0.455969388
108468	-0.145315929	-0.444430981
108473	0.029865299	-0.449249753
108598	-0.572895854	-0.212010906
108736	-0.290682073	-0.559797125
109012	0.01652971	-0.282585342
109086	-0.079595916	-0.548710969
109110	0.121589072	-0.38752598
109144	-0.109774045	-0.598889097
109207	0.125161795	-0.223953258
109214	-0.051146803	-0.470261855
109266	-0.232532709	-0.481647761
109378	0.097298534	-0.271816519
109381	0.064119487	-0.334995565
109450	nan	-0.44709474
109650	-0.179339285	-0.448454337
109795	0.088342418	-0.460772635
109821	-0.241654482	-0.450769535
110028	0.088974031	-0.390141021
110035	-0.213513169	-0.502628222
110084	-0.114820427	-0.243935479
110102	-0.149566125	-0.458681177
110109	-0.204842831	-0.413957884
110341	-0.221055946	-0.640170999
110454	-0.055882839	-0.394997891
110468	-0.564337001	-0.183452053
110512	-0.224908663	-0.444023715
110712	-0.015643004	-0.424758057
110843	0.151311227	-0.307803826
111274	0.034815377	-0.324299676
111312	-0.144584748	-0.2636998
111517	-0.041716088	-0.330831141

APPENDIX A. NLTE K ABUNDANCES AND CORRECTIONS

HIP	NLTE K	NLTE Correction
111565	-0.299837367	-0.348952419
111648	-0.263737629	-0.242852681
111746	-0.360046518	-0.439161571
111978	0.075432533	-0.21368252
112151	-0.308652966	-0.347768018
112201	0.091248942	-0.32786611
112243	-0.114355596	-0.333470648
113044	-0.012668814	-0.631783867
113113	-0.061669652	-0.300784704
113137	0.135142948	-0.413972104
113174	0.1888935	-0.580221553
113357	0.129650872	-0.32946418
113386	0.010747088	-0.398367965
113421	0.187318614	-0.291796438
113454	-0.242437214	-0.361552267
113543	-0.212742772	-0.621857824
113677	0.040179759	-0.268935294
113688	-0.187688838	-0.48680389
113777	-0.074693247	-0.173808299
114040	0.078296258	-0.300818794
114333	-0.066827901	-0.395942954
114450	-0.061227326	-0.410342379
114460	-0.108773232	-0.287888285
114576	0.043933104	-0.395181949
114584	-0.097309652	-0.356424705
114590	0.216750168	-0.352364884
114615	-0.052406735	-0.391521787
114702	-0.392603585	-0.601718637
114709	-0.186262448	-0.4853775
114743	0.000554908	-0.288560144
114761	-0.702368639	-0.651483691
114962	-1.675541532	-0.584656584
115286	0.030797076	-0.418317977
115411	-0.417236187	-0.326351239
115577	-0.050969103	-0.420084155
115662	0.027395911	-0.381719141
115792	0.150834492	-0.578280561
115803	0.021946124	-0.587168929
115861	0.144745965	-0.344369087
115917	-0.4001567	-0.519271753
116033	-0.180197294	-0.569312346
116410	-0.3545862	-0.323701253

APPENDIX A. NLTE K ABUNDANCES AND CORRECTIONS

HIP	NLTE K	NLTE Correction
116421	-0.178366728	-0.427481781
116478	-0.037217528	-0.316332581
116740	0.164313469	-0.344801583
116906	-0.207455482	-0.576570535
117320	0.129997019	-0.359118033
117364	-0.069064706	-0.398179758
117526	0.157955684	-0.251159369
117627	-0.096955045	-0.276070098
117880	0.047936394	-0.521178658
117902	0.067417446	-0.321697606
117961	0.10600892	-0.333106132
118010	-0.045754986	-0.454870039
118115	-0.018064164	-0.387179217
118141	-0.249129567	-0.61824462
118143	-0.054729709	-0.303844761